Modular Organization of Electrical Fluctuations in the Mouse Brain

Xingyun Wang[2, 3, 4], Jean-Claude Béïque[2, 3, 4], and Richard Naud[1, 2, 3, 4 *]

[1]Department of Cellular and Molecular Medicine, University of Ottawa
[2]Department of Physics, University of Ottawa
[3]Center for Neural Dynamics and Artificial Intelligence, University of Ottawa
[4]University of Ottawa Brain and Mind Research Institute University of Ottawa
[*]Corresponding author: rnaud@uottawa.ca

November 21, 2025

Abstract

A powerful computational feature of the brain is its ability to compartmentalize different functions in a way that can be flexibly recombined. Experimental evidence for such modularity arose from cytoarchitecture, connectivity, and electroencephalograms, while magnetic resonance imaging could attest that this modularity is dynamic. More spatially precise and more widely recordable, the local field potential (LFP) has an unknown brain wide organization. Here, we developed deep electrospectroscopy, a method to assess nonlinear spectral similarity between the LFP of different areas. A brain-wide application of this technique to the mouse brain revealed an organization composed of groups of spectrally similar areas. Such communities were mostly found in the forebrain and showed an organization that did not strictly follow the cytoarchitecture. For instance, visual parts of the cortex and the visual parts of the colliculus were found in the same community. These electrospectral communities reshaped with context, showing splitting and merging operations, growing in size around brain areas required for a task. In particular, upper and lower limb parts of the somatosensory cortex were primarily in separate communities but merged during a task that required turning a wheel. Similarly, oculomotor reflexes and associative parts of the thalamus merged during the visuo-motor task. These analyzes show that LFPs are organized in a modular fashion, offering a window onto subcortical and layer-specific contributions to the compositionality of cortical brain functions.

Introduction

Recent brain-wide recordings of activity have made clear that every part of the brain encodes almost every aspect of the world to some degree [1, 2]. These observations come as a puzzle if one consider the brain as a set of separated modules feeding into a centralized control of behavior [3]. Cognitive science and artificial intelligence investigations have proposed modules work in parallel [4], that motor control forms hierarchies [**?**], and that modules can reconfigure into compound functions [5, 6]. How does such a modular reconfiguration take place in the brain is therefore a central question in neuroscience. Brain modularity is observable in patterns of similarities and dissimilarities across different brain areas [7, 8]. Focusing on activity-related signals, coarse modules were found in brain-wide electroencephalograms (EEGs) and in functional magnetic resonance imaging (fMRI) [9, 10]. These modules were shown to be highly similar to the modules found in patterns of traced connectivity data [11], suggesting that the modular structure of brain connectivity is echoed by its connectivity. Studies in mice could further probe the question of what underlies this modularity. A modular organization was found in the cytoarchitecture, connectivity and transcriptome [12, 13, 14]. Yet, the recordings focused on cortex and often lacked both dynamics and layer precision. A picture of how modules reconfigure the different layers of cortical and subcortical elements is lacking.

With recent developments in silicon probes [15, 1, 16], local field potentials (LFPs) can, in principle, be recorded with high-density, and deep structures can be reached. Offering a microscopic picture of the electrical fluctuations across almost the entire mouse brain [17, 18], this signal is thought to reflect

a mixture of activity patterns from afferents and the local population [19]. Synchronized afferent patterns, traveling waves, and inter-area synchronization [20, 21, 22, 23] are specific activity patterns that shape the LFP and can endow it with a modular structure. Yet, while many location-specific LFP patterns have been found [24, 25, 26, 27, 28, 29, 30, 31, 32, 33, 34, 35], little is known about how the LFP is organized across the entire brain, let alone whether its organization is modular.

Here, we reasoned that patterns of similarity could be found in the spectrograms of the LFP recorded across almost the entire mouse brain, but that these patterns may require analysis methods more perceptive than the correlation coefficient. This article is constructed in two sections. First, we trained deep artificial networks to localize LFPs, integrating possibly nonlinear relationships between features of the LFP and brain areas. Second, we use this model to assess the similarity and dissimilarity of areas, and thus to reveal the presence, structure and task-dependence of modules.

Results

We used publicly available, multi-lab, brain wide Neuropixels recordings (International Brain Lab; IBL [17, 18, 36, 2]). In this standardized dataset, mice were cued with an auditory tone and a visual grating to steer a wheel. For each trial and for each channel, we extracted the spectrogram from one second of LFP recordings taken during the inter-trial time period and at the onset of the task (Fig. 1a). The use of LFP spectrograms, or electrospectra, preserved some information about interactions between timescales, about transient synchronization to task features and about nearby multi-unit activity [37]. After quality control and shaping the data for our purposes (see Methods), we obtained LFPs from 472 different brain regions across 127 animals and 12 labs, for a total of 1 687 471 independent LFP segments (samples) taken during the intertrial period. While we present our analysis of this inter-trial period first, we will later present an analysis the other 1.7 M samples taken during the task period.

Nonlinear features of the LFP enable milimetric localization

As a preliminary investigation, we inquired about the spatial scale of changes in the electrospectra. A previous study has estimated the autocorrelation length (equivalent to the positional error of a linear model) of LFPs to a tenth or a third of the rostrocaudal length [38], depending on brain state. We therefore asked if using a method that can extract electrode positions from a nonlinear combinations of electrospectral features could do so with more precision than the average autocorrelation length. Accordingly, we trained deep networks (see Methods) in this task using samples from the inter-trial period and electrode position estimated using stereotaxis (Supplementary Fig. 2). We found positional error between 5 and 9 % of brain length, depending on axis (standard deviation of regression residuals 0.7-1.2 mm, compared to brain length of 14 mm). While preliminary, this observation supports the idea that our deep networks reveal a more precise structure than linear methods.

Since we are interested in the relationship between brain areas rather than raw positions, we then trained our networks to predict the source brain area for every sample [39] (Fig. 1a). To ensure reproducibility, we considered three different classifiers: a deep network developed for sound classification (AnyNet; [40]), a visual transformer (ViT; [41, 42]) and a recurrent neural network (RNN; [43]; Suppl. Fig. 1). Data was separated into a training set, a validation set and two test sets. One test set was made of different trials from the same animals used for training (cross-trial test), and the other test set was composed of different animals (cross-subject test; Fig. 1c), allowing us to test different types of generalization. We computed the average cross-trial accuracy for the three neural networks, along with a linear classifier. While a linear classifier was able to localize electrodes far better than chance (accuracy of 0.120 vs 0.002 for chance), its accuracy was surpassed by each of the three deep learning networks (Fig. 2a). Among these, performances were of the same order, with a small advantage for the ViT (0.389) and a small disadvantage for the RNN (0.312) and AnyNet midway (0.368). Therefore, deep learning captures combinations of features in the electrospectra that were not captured using linear methods.

To gain insights on the type of features exploited by the models, we also trained our models to classify time-averaged spectra instead of time-resolved spectrograms (Suppl. Fig. 3). In this case, the linear classifier upkept its accuracy (0.119), but the accuracy of the deep models dropped (AnyNet 0.213, ViT 0.357, RNN 0.176). This indicates that information increases from linear features

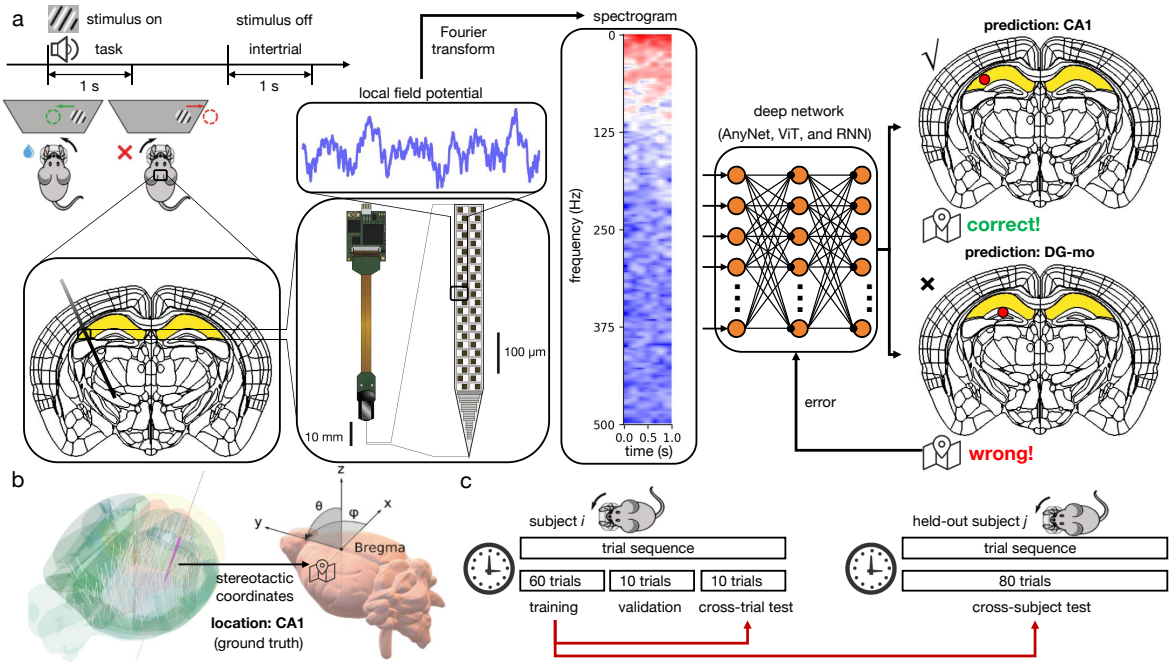

Figure 1: **Deep learning LFP localization a.** Workflow schematic for brain area classification. Opensource Neuropixels data from the IBL was used for both task and intertrial states of a period of 1 second. We used LFP recorded during the inter-trial period. Each LFP on each electrode in each session was converted to a spectrogram and fed to an ANN (ViT, AnyNet or RNN) for localization. The ANN parameters were learned based on correct and erroneous prediction of the brain area of the recording, as illustrated here with a recording localized in cornu ammonis 1 (area 'CA1') but that could have been predicted to lie in the dentate gyrus ('DG-mo'). **b.** The ground truth of a recording's location were obtained by mapping its stereotaxis coordinates to a histologically-defined brain atlas (Allen Brain or Cosmos). **c.** Schematic of training and different test sets. For the first experiment of each subject except held-out subjects, we used first 60 trials to train and the following 10 trials for validation. The last 10 trials from each subject were were used to quantify the cross-trial test. The first 80 trials of held-out subjects consisted of the cross-subject test. Cross-trial and cross-subject tests correspond to in-distribution and out-distribution tests in machine learning.

to nonlinear feature combinations of the time-averaged spectra, and increases further with nonlinear feature combinations of spectrograms.

Deep learning reveals multiple electrospectral landmarks

We then asked what makes one area more recognizable than another. Plotting the accuracy area-by-area (Fig. 2b,c), we found a considerable variability. We performed a multivariate regression of the region-specific accuracy on four factors: i) the volume of the brain area, ii) the number of samples (Fig. 2d), iii) the recording depth, which could decrease the accuracy via an increased stereotactic error but could also indicate more recognizable deeper structures either intrinsically or by bearing less artifacts of the surgery, and iv) the number of subjects. We found that the main factors affecting the cross-trial accuracy are the volume and the sample number, while the depth and subject numbers have comparatively negligible contributions (Fig. 2d). Surprisingly, depth was positively associated with accuracy, suggesting that stereotaxis errors are small and deeper are more recognizable. These factors, however, could not account for the majority of the variability (regression R^2=0.14). Therefore, the considerable variability in localization accuracy is not fully accounted for by the size and number of samples and supports the idea that some areas are intrinsically more recognizable than others.

We call those more recognizable areas 'landmarks'. Examples from the cross-trial test are the main olfactory bulb (MOB), cornus ammonis 1 (CA1) and the different layers of the dentate gyrus (DG; Fig. 2b,c). Turning to the cross-subject test, here we expect that variability in brain morphologies

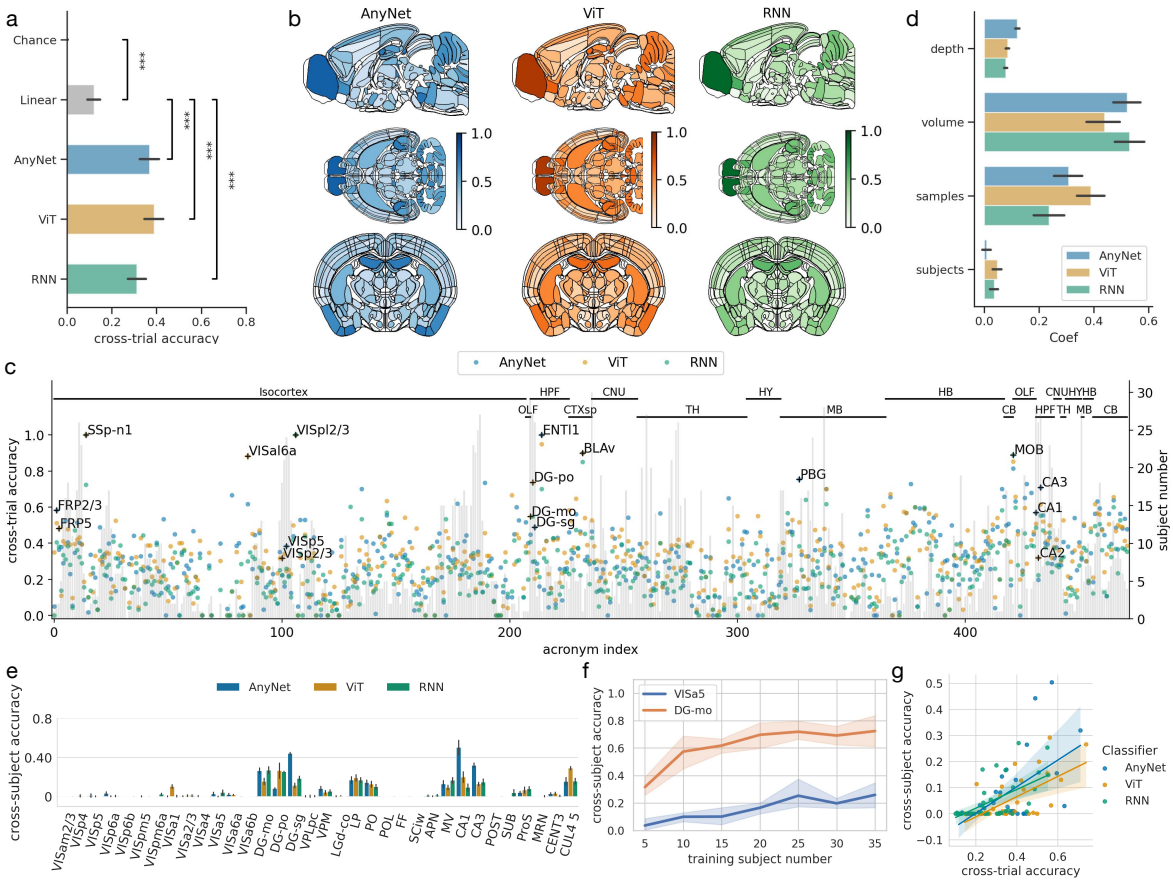

Figure 2: **Electrospectral landmarks show high accuracy across trials and subjects a.** Overall cross-trial accuracy from distinct classifiers: linear network model, AnyNet, ViT, and RNN. Linear classifier performs significantly better than the chance level ($p < 0.001$). The three deep networks (AnyNet, ViT, and RNN) outperform the linear classifier ($p < 0.001$). **b.** Beta coefficients of multi-linear regression of cross-trial accuracy against depth, volume, samples and number of subjects. **c.** Spatial distribution of individual cross-trial accuracy from three classifiers across the mouse brain. **d.** Individual cross-trial accuracy (left axis) of the three deep learning models for the 472 brain regions. At the top of the figure is the label of the anatomical divisions. The subject number of each brain region is shown as gray bars referring to the right-axis. **e.** Cross-subject accuracy for brain areas having at least have 10 subjects. **f.** AnyNet cross-subject accurcay while holding out 5 subjects and gradually increasing the subject number in the training dataset. **g.** Scatter plot of cross-subject against cross-trial accuracies. Pearson Correlation between cross-trial accuracy and cross-subject accuracy are AnyNet $r = 0.587$, $p = 0.00027$; ViT $r = 0.334$, $p = 0.0537$; RNN $r = 0.501$, $p = 0.00252$. See Supplementary Table 1 for acronym definition.

will necessarily reduce the maximal accuracy. Also, since most areas were not sampled consistently across animals, we could only perform this cross-subject test for a fraction of the areas (see Methods). Cross-subject accuracies for the remaining areas are shown in Figure 2e. A number of cross-subject landmarks can be identified by virtue of their relatively high accuracy. These include CA1, CA3 and each of the three layers of the DG. Other than these areas known for their distinctive LFP, we found the lateral posterior nucleus (LP), the posterior complex (PO) of the thalamus, hindbrain's medial vestibular nucleus (MV) and the cerebellum's Lobule IV (CUL4 5).

Given the added difficulty of the cross-subject test, it remains possible that these accuracies mainly reflect the number of subjects. To verify this, we selected two areas, non-landmark VISa5 (visual cortex, anterior area, layer 5) and landmark DG-mo (dentate gyrus, molecular layer), and gradually increased the subject number in the training set while testing in held-out subjects (Fig. 2f). As expected, the accuracy gradually increased with the number of animals in the training set. Yet, VISa5 required 35

subjects to match the accuracy achieved by DG-mo with only 5 subjects, further supporting that DG-mo is a landmark of the LFP. To more broadly test whether a landmark identified in cross-trial tests is predictive of landmark status in cross-subject tests, we calculated the correlation between cross-trial and cross-subject accuracies (Fig. 2g). We found a positive correlation, thus supporting the idea that we can identify subject invariant electrospectral structure from cross-trial tests.

Electrospectral localization transfers to human

We further investigated the idea that our models trained on mice can then be fine-tuned on limited data to localize LFP from human brains, indicating a shared electrospectral structure across species. To investigate this, we used a human Neuropixels dataset, which was recorded from the dlPFC and temporal lobe [16]. In the absence of a precise mapping to a coordinate framework, we considered 21 labels based on electrode identity and used our three classifiers as we did for mice. We compared two training approaches: i) training classifiers from randomly initialized weights on the human dataset and ii) training classifiers that were pre-trained on the large mice dataset while only allowing the penultimate layer weights to be changed. If there is a shared structure across species, we should observe a faster learning in the pre-trained group. The final accuracy, in contrast, is more likely to reflect the restriction of which weight is allowed to be trained. We found that classifiers pre-trained with mice data could learn much faster than their counterparts trained from a random initialization on the human dataset (Suppl. Fig. 4). The final cross-trial accuracy did not show a significant difference between the transfer learning and random initialization group. This result further supports the potential for generalization of the electrospectral features learned by the models.

Electrospectral similarities reveal robust communities

Inspired by spectroscopy approaches that rely on spectral matching to identify the composition of a sample, we hypothesized that a group of areas may share electrospectral features even when LFP spectra do not show well-separated peaks. Because the relevant spectral features may mix nonlinearly, we rely on the ANN representations of electrospectra rather than the electrospectra to assess similarity (Suppl. Fig. 5a). We found that the three ANNs converged to a consistent similarity matrix (Suppl. Fig. 5b).

We thus applied an approach from graph theory to delineate shared spectral features. The generalized modularity index [44] uses the ANN's confusion matrices to create an undirected weighted graph and then quantifies the degree to which a given community structure is unlikely to arise from a random graph. The index is defined with a hyperparameter called the resolution (see Methods), which biases towards big communities when small. Given a resolution parameter, we used a greedy modularity search [45] to find a clustering that maximizes modularity (Suppl. Fig. 5c). Furthermore, to ensure that we find a community structure that does not depend on the specific ANN architecture, we performed the modularity search on each network independently and then focused on areas that are at the intersection between the communities found using each classifier (Fig. Suppl. 5d), the ensemble communities.

Before diving into the structure of the resulting electrospectral atlas, we explored different resolution parameters. Suppl. Fig. 5e shows the optimal modularity as a function of resolution. As a rule-of-thumb for modularity-based approaches, the index should be higher than 0.3 [9, 46], which is achieved for resolutions higher than 0.5. As higher resolutions yield smaller communities, we checked the robustness of the communities at different resolutions by bootstrapping the similarity matrix (Suppl. Fig. 5f) and found a monotonically decreasing robustness with an overlap ratio at 75% when using a resolution of 1. We also computed the cross-trial and cross-subject accuracies for the classifications of communities found at different resolutions (Suppl. Fig. 5g-h). Here the resolution showed only a small effect on robustness, and only the non-modular resolution (0.4) was markedly more robust, an observation explained by the very large communities that bias the accuracy due to class imbalance (Suppl. Fig. 6a). The localization accuracies of communities matched those of the areas that were individually most recognizable (landmark areas in Fig. 2). The resolution parameter therefore controls a trade-off between low robustness and low modularity, such that a resolution of one offers a good compromise.

Next we sought to compare the localization accuracies of an atlas based on the electrospectral communities and one based on a coarse histological atlas. We thus trained our classifiers on an

atlas of ten mouse brain regions (e.g. olfactory bulb, isocortex, see Fig. 3b). Referring to this map as the Cosmos Atlas [17], we found again that a linear classifier was more apt than chance but surpassed by deep networks (Suppl. Fig. 5i, Suppl. Fig. 7). The deep networks achieved a cross-trial accuracy around 0.65. We could then directly compare the Cosmos Atlas with the 10 most recognizable communities, thus matching the task difficulty. We found that even when separating the brain into smaller regions than Cosmos, it is easier to localize communities of the electrospectral atlas (Suppl. Fig. 5j).

Electrospectral communities of the intertrial period

Focusing on a selected set of communities, Figure 3 shows the resulting network graph with communities denoted by different colors (see also exemplar spectrograms in Suppl. Fig. 8 and full list in Suppl. Table 1). We stress that the links in the graph denote spectral similarity, not synaptic connections between areas. Graph theory analysis defines hub and connector nodes. Defining a hub node as the node with the largest in-degree, we looked at the probability that a given cortical layer was a hub (Fig. 15; Table 3). We found a layer specific probability where L6a and L5 were most likely and L4 and L6b the least likely. Performing the same analysis for connector nodes did not show a significant layer specificity (Fig. 15).

Many communities suggested an alignment with function. For instance, we found an 'audio-visual community' composed of the union of auditory cortex, parts of higher-order visual cortex, temporal and parietal association areas, a 'hippocampus community' which regrouped CA1, CA2, CA3 with entorhinal cortex, the 'olfactory community' regrouped parts of the olfactory bulb with frontal pole and orbitofrontal cortex, or a 'visuo-vibrissal community' that unites lateral and anterior visual cortex with temporal association areas and barrel fields. The area at the top of the visual hierarchy [13], labeled 'VISam', formed a relatively isolated community. The alignment with function was also suggested by subcortical communities such as a 'auditory reflexes community', which united superior olive (SOCI), inferior colliculus (ICc), a nucleus for the acoustic startle response (PRNc), and one for the tensor tympanic muscle (PC5). The 'amygdala community' regrouped the lateral amygdalar nucleus (LA) with the piriform amygdalar area of the olfactory bulb (PAA) and the cortical amygdalar area (COA). Alignment with function was not manifest for all communities, such as the large 'cerebellum-hindbrain' community, or the union of three small and tegmental areas we called 'raphe' (Fig. 3a).

At times, however, communities were not strictly circumscribed by the broad cytoarchitectural regions of the brain (Fig. 3b). For example, the putamen was the hub node of a community that unites nucleus accumbens, gustatory cortex, parts of the motor, somatosensory, anterior cingulate and insular cortex. Because many of these areas are part of the cortico-basal-ganglia loop, receiving inputs from the parafascicular nucleus, we labeled this community 'motor planning'. The layer resolution of the LFP allowed to match specific layers of the colliculus with layers of the cortex: The 'core visual community' contained the optic parts of colliculus, primary visual cortex, parts of retrosplenial cortex and area prostriata, but not many other associative parts of the visual cortex, nor the other layers of the colliculus. The motor parts of the superior colliculus were instead separated into two communities (Suppl. Fig. 10), one containing many hypothalamic areas, and the other containing oculomotor parts of the midbrain. Therefore, we find that electrospectral communities can deviate from the cytoarchitecture in a way that suggests an alignment with function.

Electrospectral communities reshape according to the task

To establish the community structure in a different context, we used the other set of models trained on the 1.7 M LFP samples of the task period. The IBL task required visual and auditory acuity, lower and upper limb coordination for turning a wheel and licking for obtaining rewards [18, 36, 2]. The communities were established anew using the same resolution parameter (Fig. 3c, exemplar spectrograms in Suppl. Fig. 9, and subsystems task-intertrial comparisons in Suppl. Fig. 10 - Fig. 13). We found that some communities appeared (a union of lower and upper limbs), some disappeared (visuo-vibrissal, visuo-tactile), some communities stayed approximately the same (visuo-auditory, visual-am, septal nuclei, amygdala) and others reshaped by adding or removing areas for a set of core areas.

Consistent with the appearance of the drifting grating, vision-related communities showed much reshaping. The core visual community increased in size (17 areas in the intertrial period vs. 25 in

the task), with the inclusion of visual areas VISpm and VISa and reducing areas from VISli and VISl. The visual parts of the colliculus and area prostriata remained in this community, which also remained centered on layer 5 of the primary visual cortex (VISp5). Plotting the network graph of all communities containing subcortical visual and auditory areas (Suppl. Fig. 10), we observed that SCsg (a visual layer of superior colliculus) preserved some similarity with SCiw (intermediate white layer). SCiw belongs to a large community that contains motor and association parts of the superior colliculus along with most of midbrain (including oculomotor areas) and a large portion of thalamus, a merger of two communities of the intertrial period. To verify that this merge was significant, we performed a bootstrap test on probability of selected areas to be in the same or a different community (Fig. 4b, see Graph Theory Methods). Interestingly, a new small community appeared that contained both the visual and auditory relay thalamus despite these areas being dominated by categorically different afferents. These relay areas did not belong to any community during the intertrial period. Together, the picture that arises is that much reshaping of communities took place, both in terms of cortical and subcortical areas, at least around areas connected to the task.

Potentially reflecting the licking and wheel-maneuvering components of the task, we found that motor and planning areas were marked by a split. During the intertrial period, the motor planning community centered on the putamen and contained the nucleus accumbens (ACB), frontal pole (FRP), anterior cingulate area (ACA), the secondary motor cortex (MOs), agranular insula (AI) , primary motor cortex and orofacial somatosensation (SSp-n, SSp-m). During the task, putamen was still part of the community that integrated ACA, MOs and ACB, but the orofacial and primary motor areas formed a distinct community. We performed a bootstrap test to verify the significance of this split (Suppl. Fig. 5c). Interestingly, while most similar to the hippocampus or the septal nuclei community during the inter-trial state, the motor planning community became most similar with the visual and limbs communities. Together, these findings support that the LFP is organized in modules which can reconfigure with behavior.

Discussion

Brain-wide brain wide graphs of Suppl. Fig. 5 and 3 appear centered on the caudoputamen, a subcortical structure involved in motor control, emotion and cognition. Graphs that contain such hub structure are naturally highly sensitive to subsampling. Therefore, we expect that an even wider sampling of areas can alter the precise hierarchical graph that can be inferred from the LFP. Similarly, there different hyperparameters or different modularity search will likely provide a slightly different community structure.

The default mode network is a group of areas identified in humans that are active specifically during the resting state. One may ask if any of the electropectral communities matches the mouse DMN. Following Whitesell et al. (2021) [**?**], the cortical part of mouse core DMN regroups areas along the midline (ACAd, ACAv, PL, ILA, ORBl, ORBm, ORBvl, VISa, VISam, RSPd, RSPv, SSp-tr, SSp-ll and MOs). Except for the sensory areas (RSP, SSp and VIS), these areas are all found in the motor planning community. Therefore, the largest cortical community aligns substantially with the default mode network. This community splits during the task, when the default mode network is inhibited.

Given that the LFP is shaped by both the activity patterns of the afferents and those in the local population [19], one may ask if either of those factors influence more the community structure. If the structure of the LFP was dominated by afferents, we would expect that the electropectral community should reflect the modularity of the connectivity. Previous research has revealed community structure in the connectivity of intracortical connections [13, 12], and these clearly show a high degree of overlap with the electrospectral communities. If, alternatively, the LFP was dominated by local properties, we would expect that the local transcriptome would reflect the modularity of the electrospectra. Again here, the modularity structure of the local transcriptome shows a high overlap with that of the LFP. While these comparisons are ambiguous, it is worth to note that our findings indicate a dynamical structure of the LFP. Within the connectivity and cytoarchitectural constraints, the LFP re-organizes with the behavior, with layer precision, both across cortex and subcortical structures.

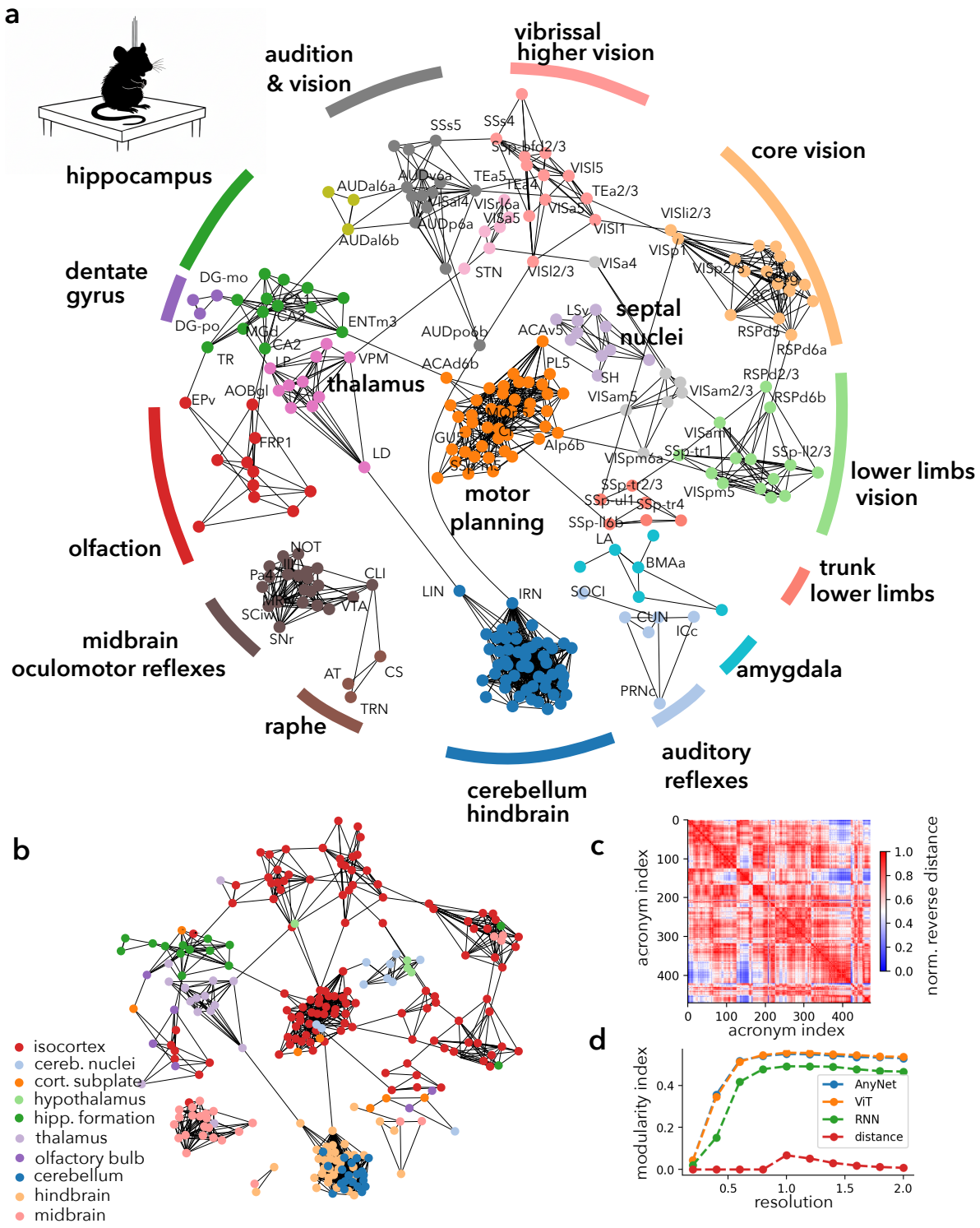

Figure 3: **Electrospectral communities during the inter-trial period.** **a** A selection of electrospectral communities (different colors) identified during the inter-trial state. Each circle represent an Allen atlas area. Graph links represent thresholded elements of the confusion matrix, with thicker lines corresponding to higher values of the confusion matrix. **b** Same graph as panel a, but colors representing coarse histological atlas. **c** Matrix of reversed normalized distances between area centers. **d** Comparison of modularity indices with the deep learning algorithms on electrospectra with those obtained from distances between areas centers. The modularity index mean and standard deviation are obtained by bootstrapping. Standard deviations are not visible because they are smaller than the marker size.

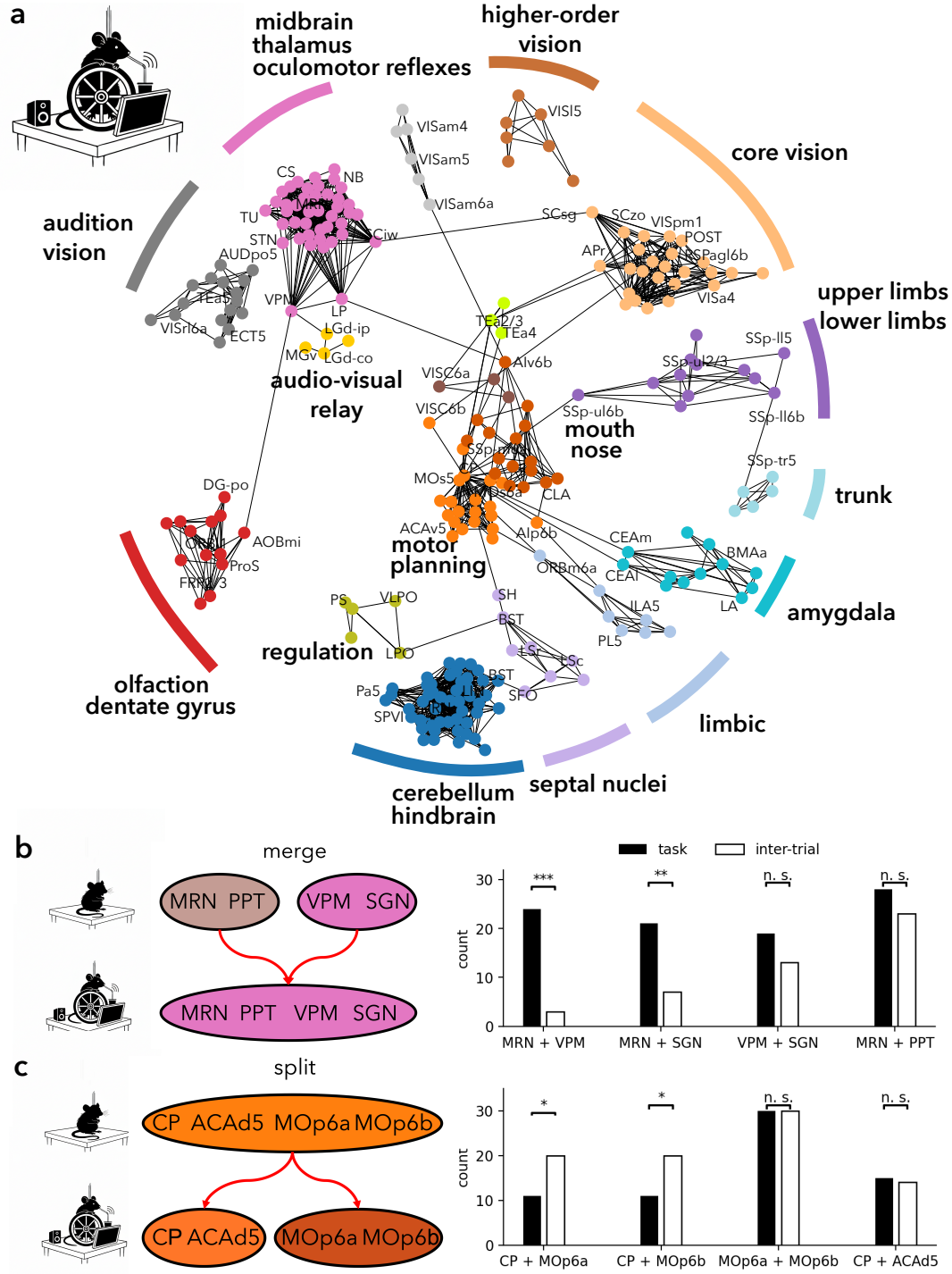

Figure 4: **Electrospectral modules recombine during the task.** **a** A selection of communities obtained during the visuo-motor task, as in Fig. 3. **b** Bootstrap test using Fisher's exact method for computing the probability that two communities are in the same community in the task (black bar) and during the intertrial period (white bar). The MRN is in the same community as PPT but not VPM nor SGN during the intertrial period, while it is also in the same community as VPM and SGN in the task period, indicating a merge of communities in the task period. **c** Same as b, but for areas CP, ACAd, MOp6a and MOp6b, indicating a split of communities in the task period.

References

[1] Nicholas A Steinmetz, Cagatay Aydin, Anna Lebedeva, Michael Okun, Marius Pachitariu, Marius Bauza, Maxime Beau, Jai Bhagat, Claudia Böhm, Martijn Broux, et al. Neuropixels 2.0: A miniaturized high-density probe for stable, long-term brain recordings. *Science*, 372(6539):eabf4588, 2021.

[2] Charles Findling, Felix Hubert, International Brain Laboratory, Luigi Acerbi, Brandon Benson, Julius Benson, Daniel Birman, Niccolò Bonacchi, E Kelly Buchanan, Sebastian Bruijns, et al. Brain-wide representations of prior information in mouse decision-making. *Nature*, 645(8079):192–200, 2025.

[3] Jerry A Fodor. Precis of the modularity of mind. *Behavioral and brain sciences*, 8(1):1–5, 1985.

[4] David E Rumelhart, James L McClelland, PDP Research Group, et al. *Parallel distributed processing, volume 1: Explorations in the microstructure of cognition: Foundations*. The MIT press, 1986.

[5] Francis Jeffry Pelletier. The principle of semantic compositionality. *Topoi*, 13(1):11–24, 1994.

[6] Dieuwke Hupkes, Verna Dankers, Mathijs Mul, and Elia Bruni. Compositionality decomposed: How do neural networks generalise? *Journal of Artificial Intelligence Research*, 67:757–795, 2020.

[7] Bayanne Olabi, Ian Ellison-Wright, Andrew M McIntosh, Stephen J Wood, Ed Bullmore, and Stephen M Lawrie. Are there progressive brain changes in schizophrenia? a meta-analysis of structural magnetic resonance imaging studies. *Biological psychiatry*, 70(1):88–96, 2011.

[8] Jinseop S Kim and Marcus Kaiser. From caenorhabditis elegans to the human connectome: a specific modular organization increases metabolic, functional and developmental efficiency. *Philosophical Transactions of the Royal Society B: Biological Sciences*, 369(1653):20130529, 2014.

[9] David Meunier, Renaud Lambiotte, Alex Fornito, Karen Ersche, and Edward T Bullmore. Hierarchical modularity in human brain functional networks. *Frontiers in neuroinformatics*, 3:571, 2009.

[10] Olaf Sporns and Richard F Betzel. Modular brain networks. *Annual review of psychology*, 67(1):613–640, 2016.

[11] Christopher J Honey, Rolf Kötter, Michael Breakspear, and Olaf Sporns. Network structure of cerebral cortex shapes functional connectivity on multiple time scales. *Proceedings of the National Academy of Sciences*, 104(24):10240–10245, 2007.

[12] Brian Zingg, Houri Hintiryan, Lin Gou, Monica Y Song, Maxwell Bay, Michael S Bienkowski, Nicholas N Foster, Seita Yamashita, Ian Bowman, Arthur W Toga, et al. Neural networks of the mouse neocortex. *Cell*, 156(5):1096–1111, 2014.

[13] Julie A Harris, Stefan Mihalas, Karla E Hirokawa, Jennifer D Whitesell, Hannah Choi, Amy Bernard, Phillip Bohn, Shiella Caldejon, Linzy Casal, Andrew Cho, et al. Hierarchical organization of cortical and thalamic connectivity. *Nature*, 575(7781):195–202, 2019.

[14] Xiaoyin Chen, Stephan Fischer, Mara CP Rue, Aixin Zhang, Didhiti Mukherjee, Patrick O Kanold, Jesse Gillis, and Anthony M Zador. Whole-cortex in situ sequencing reveals input-dependent area identity. *Nature*, pages 1–10, 2024.

[15] James J Jun, Nicholas A Steinmetz, Joshua H Siegle, Daniel J Denman, Marius Bauza, Brian Barbarits, Albert K Lee, Costas A Anastassiou, Alexandru Andrei, Çağatay Aydın, et al. Fully integrated silicon probes for high-density recording of neural activity. *Nature*, 551(7679):232–236, 2017.

[16] Angelique C Paulk, Yoav Kfir, Arjun R Khanna, Martina L Mustroph, Eric M Trautmann, Dan J Soper, Sergey D Stavisky, Marleen Welkenhuysen, Barundeb Dutta, Krishna V Shenoy, et al. Large-scale neural recordings with single neuron resolution using neuropixels probes in human cortex. *Nature Neuroscience*, 25(2):252–263, 2022.

[17] Larry F Abbott, Dora E Angelaki, Matteo Carandini, Anne K Churchland, Yang Dan, Peter Dayan, Sophie Deneve, Ila Fiete, Surya Ganguli, Kenneth D Harris, et al. An international laboratory for systems and computational neuroscience. *Neuron*, 96(6):1213–1218, 2017.

[18] International Brain Laboratory, Valeria Aguillon-Rodriguez, Dora Angelaki, Hannah Bayer, Niccolò Bonacchi, Matteo Carandini, Fanny Cazettes, Gaelle Chapuis, Anne K Churchland, Yang Dan, et al. Standardized and reproducible measurement of decision-making in mice. *Elife*, 10:e63711, 2021.

[19] György Buzsáki, Costas A Anastassiou, and Christof Koch. The origin of extracellular fields and currents—eeg, ecog, lfp and spikes. *Nature reviews neuroscience*, 13(6):407–420, 2012.

[20] Pieter R Roelfsema, Andreas K Engel, Peter König, and Wolf Singer. Visuomotor integration is associated with zero time-lag synchronization among cortical areas. *Nature*, 385(6612):157–161, 1997.

[21] Marius Schneider, Ana Clara Broggini, Benjamin Dann, Athanasia Tzanou, Cem Uran, Swathi Sheshadri, Hansjörg Scherberger, and Martin Vinck. A mechanism for inter-areal coherence through communication based on connectivity and oscillatory power. *Neuron*, 109(24):4050–4067, 2021.

[22] Theodoros P Zanos, Patrick J Mineault, Konstantinos T Nasiotis, Daniel Guitton, and Christopher C Pack. A sensorimotor role for traveling waves in primate visual cortex. *Neuron*, 85(3):615–627, 2015.

[23] J Jesús Hernández-Pérez, Keiland W Cooper, and Ehren L Newman. Medial entorhinal cortex activates in a traveling wave in the rat. *Elife*, 9:e52289, 2020.

[24] Wolfgang Klimesch. Alpha-band oscillations, attention, and controlled access to stored information. *Trends in cognitive sciences*, 16(12):606–617, 2012.

[25] Charline Peylo, Yannik Hilla, and Paul Sauseng. Cause or consequence? alpha oscillations in visuospatial attention. *Trends in Neurosciences*, 44(9):705–713, 2021.

[26] Rosanne M Van Diepen, John J Foxe, and Ali Mazaheri. The functional role of alpha-band activity in attentional processing: the current zeitgeist and future outlook. *Current opinion in psychology*, 29:229–238, 2019.

[27] Supratim Ray and John HR Maunsell. Do gamma oscillations play a role in cerebral cortex? *Trends in cognitive sciences*, 19(2):78–85, 2015.

[28] Ole Jensen, Jochen Kaiser, and Jean-Philippe Lachaux. Human gamma-frequency oscillations associated with attention and memory. *Trends in neurosciences*, 30(7):317–324, 2007.

[29] Ole Jensen, Bart Gips, Til Ole Bergmann, and Mathilde Bonnefond. Temporal coding organized by coupled alpha and gamma oscillations prioritize visual processing. *Trends in neurosciences*, 37(7):357–369, 2014.

[30] Antonio Fernandez-Ruiz, Anton Sirota, Vítor Lopes-dos Santos, and David Dupret. Over and above frequency: gamma oscillations as units of neural circuit operations. *Neuron*, 111(7):936–953, 2023.

[31] György Buzsáki. Hippocampal sharp wave-ripple: A cognitive biomarker for episodic memory and planning. *Hippocampus*, 25(10):1073–1188, 2015.

[32] Bernhard P Staresina and Maria Wimber. A neural chronometry of memory recall. *Trends in cognitive sciences*, 23(12):1071–1085, 2019.

[33] Yuta Senzai and György Buzsáki. Physiological properties and behavioral correlates of hippocampal granule cells and mossy cells. *Neuron*, 93(3):691–704, 2017.

[34] Diego Mendoza-Halliday, Alex James Major, Noah Lee, Maxwell J Lichtenfeld, Brock Carlson, Blake Mitchell, Patrick D Meng, Yihan Xiong, Jacob A Westerberg, Xiaoxuan Jia, et al. A ubiquitous spectrolaminar motif of local field potential power across the primate cortex. *Nature Neuroscience*, 27(3):547–560, 2024.

[35] Tianxiao He, Malhar Patel, Chenyi Li, Anna Maslarova, Mihály Vöröslakos, Nalini Ramanathan, Wei-Lun Hung, Gyorgy Buzsaki, and Erdem Varol. Self supervised learning for in vivo localization of microelectrode arrays using raw local field potential. In *The Thirty-ninth Annual Conference on Neural Information Processing Systems*.

[36] Dora Angelaki, Brandon Benson, Julius Benson, Daniel Birman, Niccolò Bonacchi, Kcénia Bougrova, Sebastian A Bruijns, Matteo Carandini, Joana A Catarino, et al. A brain-wide map of neural activity during complex behaviour. *Nature*, 645(8079):177–191, 2025.

[37] Gemechu Bekele Tolossa, Aidan M Schneider, Eva Dyer, and Keith B Hengen. Neurons throughout the brain embed robust signatures of their anatomical location into spike trains. *eLife*, 13:RP101506, 2025.

[38] Alain Destexhe, Diego Contreras, and Mircea Steriade. Spatiotemporal analysis of local field potentials and unit discharges in cat cerebral cortex during natural wake and sleep states. *Journal of Neuroscience*, 19(11):4595–4608, 1999.

[39] Susan M Sunkin, Lydia Ng, Chris Lau, Tim Dolbeare, Terri L Gilbert, Carol L Thompson, Michael Hawrylycz, and Chinh Dang. Allen brain atlas: an integrated spatio-temporal portal for exploring the central nervous system. *Nucleic acids research*, 41(D1):D996–D1008, 2012.

[40] Ilija Radosavovic, Raj Prateek Kosaraju, Ross Girshick, Kaiming He, and Piotr Dollár. Designing network design spaces. In *Proceedings of the IEEE/CVF conference on computer vision and pattern recognition*, pages 10428–10436, 2020.

[41] Ashish Vaswani, Noam Shazeer, Niki Parmar, Jakob Uszkoreit, Llion Jones, Aidan N Gomez, Łukasz Kaiser, and Illia Polosukhin. Attention is all you need. *Advances in neural information processing systems*, 30, 2017.

[42] Alexey Dosovitskiy, Lucas Beyer, Alexander Kolesnikov, Dirk Weissenborn, Xiaohua Zhai, Thomas Unterthiner, Mostafa Dehghani, Matthias Minderer, Georg Heigold, Sylvain Gelly, et al. An image is worth 16x16 words: Transformers for image recognition at scale. *arXiv preprint arXiv:2010.11929*, 2020.

[43] Patel Dhruv and Subham Naskar. Image classification using convolutional neural network (cnn) and recurrent neural network (rnn): A review. *Machine learning and information processing: proceedings of ICMLIP 2019*, pages 367–381, 2020.

[44] Mark EJ Newman. Modularity and community structure in networks. *Proceedings of the national academy of sciences*, 103(23):8577–8582, 2006.

[45] Aaron Clauset, Mark EJ Newman, and Cristopher Moore. Finding community structure in very large networks. *Physical Review E—Statistical, Nonlinear, and Soft Matter Physics*, 70(6):066111, 2004.

[46] David Meunier, Renaud Lambiotte, and Edward T Bullmore. Modular and hierarchically modular organization of brain networks. *Frontiers in neuroscience*, 4:200, 2010.

[47] International Brain Laboratory, Dora Angelaki, Brandon Benson, Julius Benson, Daniel Birman, Niccolò Bonacchi, Kcénia Bougrova, Sebastian A Bruijns, Matteo Carandini, Joana A Catarino, et al. A brain-wide map of neural activity during complex behaviour. *Nature*, 645(8079):177, 2025.

[48] Guido Meijer Huntenburg, Liam Paninski, Michael Schartner, Karel Svoboda, Miles Wells, Matthew R Whiteway, Olivier Winter, et al. Video hardware and software for the international brain laboratory.

[49] Alex Graves, Marcus Liwicki, Santiago Fernández, Roman Bertolami, Horst Bunke, and Jürgen Schmidhuber. A novel connectionist system for unconstrained handwriting recognition. *IEEE transactions on pattern analysis and machine intelligence*, 31(5):855–868, 2008.

[50] Aric Hagberg, Pieter J Swart, and Daniel A Schult. Exploring network structure, dynamics, and function using networkx. Technical report, Los Alamos National Laboratory (LANL), Los Alamos, NM (United States), 2008.

Supplementary Materials

Methods

International Brain Lab data

We used brain-wide Neuropixels recordings from International Brain Lab (IBL) [47], which was recorded across 139 mice in 12 labs. During the experiment, the mouse did a visual discrimination task requiring it to turn a wheel to move a visual stimulus (an oriented Gabor having variable contrasts) to the center of the screen. The mouse needed to hold the wheel still for 0.4-0.7 s to start a new trial, which was announced by an auditory cue. All mice were first trained and rewarded with sweetened water when they made correct decisions. Wrong decisions would bring a noise burst and longer inter-trial interval (2 s) as a punishment. Before the visual stimulus was turned off, the mouse had enough time for collecting the reward. Additional information for surgical methods, experimental materials, and probe tracking and alignment can be found in [18, 48]. All animal experiments were conducted according to local laws and approved by the institutional ethics committees [47]. Details for mice like housing, weights, and genders can be found in [47]. To collect samples from as many areas as possible brain areas, we used brain areas in Beryl mapping in case some recorded areas couldn't be localized precisely under the Allen brain atlas (e.g., CA1so, CA1sp and CA1sr were labeled as CA1). We didn't distinguish between hemispheres. The time period of interest was 1 second. For the intertrial period it is immediately after the visual stimulus was turned off and for the task period it is immediately after the visual stimulus was turned on. In some rare cases, the inter-trial time interval was smaller than 1 second, such that the inter-trial period contained part of this stimulus period. This only occurred on 0.06% of the trials. In all, we collected 3.4 million LFPs ($\leq$ 500 Hz) samples from 472 brain areas for 1 second in the inter-trial and the task states.

Data preprocessing

Spectrogram

For each 1 second sample of the LFP, acquired at 2500 Hz sampling frequency, we performed a Fast Fourier Transformation (FFT) with 401 bins, window length 800 sample points (320 ms), and hop of window length 400 sample points (160 ms), which results in frequency resolution of 3 Hz. We limited the frequency for analysis between 3 and 500 Hz. This results in a time-resolved spectrum (spectrogram) of dimension 224×28, where the first dimension is the frequency and the second dimension is time. We used the square root of the power so as to better preserve activity in the ripple band and beta band. This frequency range should still bear signatures of the action potentials nearby [**?**] and harmonics of rhythms slower than 3 Hz. The time-resolved spectra should also still keep partial information about rhythm nesting.

Cross validation

For each brain region, we assembled a dataset from multiple subjects. For each subject, we kept only the first 80 trials to help balance data across subjects. As a training set, we used only the first 60 trials and only for a fraction of the animals. The following 10 trials of each subject constituted the validation test. The last 10 trials of the same animals made the cross-trial test set. Some animals were held out to constitute the cross-subject test. To determine which animals were held out and which were used for the training set, we calculated the subject number for samples of each recorded brain area. We only held out subjects that would not make the sampled subject numbers for each recorded area less than 10. The cross-subject test set is then made up of the first 80 trials in the first experiment of each held-out subject.

Human data

We used publicly available Neuropixels recordings in humans, which were acquired from the dlPFC and the temporal lobe [16]. To refine the recording location, for one penetration in one coarse brain region, which had recordings from 384 channels, we only preserved one channel every 60 channels and labeled it as a new brain area index. Finally, we got 21 refined brain regions in all. All preprocessing

from LFPs to the input spectrogram of the human data was the same as mice data. For each fine brain region, we had 2 000 samples, each for 1 second. We used the first 1400 samples for training, the next 200 as validation, and reserved the last 400 for testing. In all, we had 42 000 labeled samples of human LFP.

Neural networks

Classifier architectures

The Recurrent Neural Network (RNN), the Convolutional Neural Network (CNN), and the Transformer are three basic types of modern deep network architectures. The RNN focuses on extracting sequential information with the risk of ignoring global information. The CNN extracts the local features and assembles them into a global representation by the convolution process. The self-attention mechanism in the Transformer enables the algorithm to integrate global sequential information; its quadratic computational complexity makes the training expensive.

For the RNN architecture, we treated the size of the frequency dimension of the input as the input size and the time dimension as the sequential dimension, as shown in Suppl. Fig. 6. We chose a two-layer, gated recurrent unit (GRU) module with 512 hidden units per layer. The last dimension of the output from the GRU module [49], which integrates previous sequence information, is fed into a linear layer that had the same number units as the number of brain regions. The RNN is not bi-directional because of our causal assumption of the spectrogram.

For the CNN architecture, considering the input as an image, we implemented the AnyNet framework to design our model [40]. AnyNet is a semi-auto neural architecture design framework for computer vision tasks, as shown in Suppl. Fig. 6. AnyNet consists of a stem, a body and a head. The stem was used to implement the initial processing for the spectrogram; multiple blocks exist in the body to generate the final representation by sequential nonlinear transformations; the head uses the linear readout to convert the output representation from the body to the brain region category. The architecture parameters include depth d_i, the number of the output channels c_i, the number of groups g_i, and bottleneck ratio k_i for stage i. The AnyNet design principles are the bottleneck ratio $k_i = k$, group width $g_i = g$ for all stages i; increase network width, depth across stages, which $c_i \leq c_{i+1}$, $d_i \leq d_{i+1}$. In this proposal, considering the principles and the limitations of our hardware, we designed our AnyNet as having no bottleneck and the group width is always set to be 1, in which $k_i = 1$ and $g_i = 1$; the channel number c_0 for the stem was 64, and the channel number for the remaining blocks was $c_i = c_0 * (i + 1)$; the depth for all stage was $d_i = 2$.

For the Transformer architecture, we still treated the input as an image and used the Vision Transformer (ViT) model [42], as shown in Suppl. Fig. 6. We separated the input into 8 patches, with each patch size being 28×28. A $< cls >$ token was also fed with 8 patches. After cascade transformation, its representation will be mapped into the output brain region label by a linear layer combined with the Softmax function. We implemented 8 heads and 4 Transformer encoder blocks in our ViT model.

Classifier training

As a typical method, we implemented cross-entropy to measure the loss between the label and model output for all three architectures. We used the Adam algorithm as the optimizer for training our models and set the batch size as 256. To avoid overfitting, the validation set was used for early stopping, in which we only retained models which had the best validation accuracy with training accuracy ≥ 0.6.

Computing resources

Our deep-learning based classifiers were trained by one A100 GPU. For an AnyNet classifier, training would require 4-6 hours, while for the ViT or the RNN, it required around 2 hours.

Graph Theory Methods

Greedy community search

For each classifier, we treated the confusion matrix as a weighted graph, allowing us to use theoretical tools from graph theory. To find latent communities based on the classifier's confusion matrix, we implemented Clauset-Newman-Moore greedy modularity maximization. The modularity is calculated as $Q = \frac{1}{2m}\sum_{ij}(A_{ij} - \gamma\frac{k_i k_j}{2m})\delta(c_i, c_j)$, where m is the number of edges, A is the adjacency matrix, k_i and c_i the weighted degree of node i, γ is the resolution, and $\delta(c_i, c_j)$ equals 1 when i and j are in the same community otherwise equals 0. The greedy-based method begins with each node in the graph as its own community and repeatedly merged the pairs of communities that "lead to the largest modularity until no further increase in modularity is possible (a maximum)". We performed this greedy search under different resolution (γ) conditions. We used the NetworkX package to complete above functions https://networkx.org/ [50].

Merging and splitting

To test community merge or split during distinct tasks, we examined the coexistence of chosen brain areas. We sampled 128 recordings of each brain area. (For a each brain area, if the number of samples was less than 128, we just used all samples we had). We regenerated confusion matrices 30 times. For those 30 confusion matrices, we performed greed community search as described above to obtain 30 community partitions. We counted the partitions for which the two brain areas were within the same community in task state. We repeated the computation for inter-trial states. We then used Fisher's exact test to compute the probability of rejecting he null hypothesis that there is no difference of coexistence count between two states.

Hub and connector nodes

Funding

This research was funded by CIHR Project Grant RN38364, NSERC Discovery Grant RGPIN-2024-05162 and the Brain Heart Interconnectome's Neuro-AI Platform.

Author Contributions

XW and RN designed the study, interpreted the results and wrote the manuscript. XW performed the computational analyses. JCB and RN acquired funding. RN supervised the project. JCB provided a verification of the approaches.

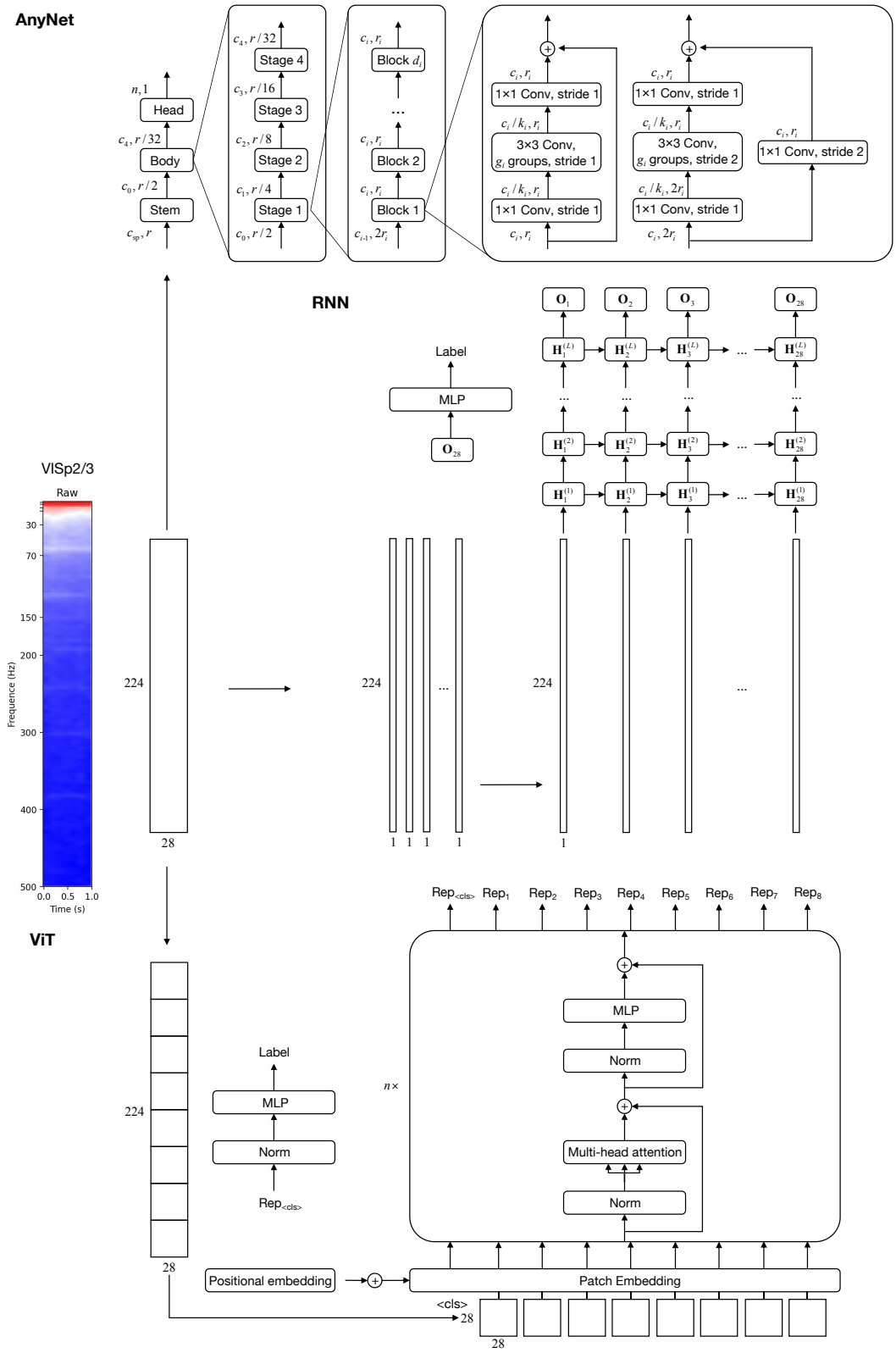

Supplementary Figure 1: **Architectures for the AnyNet, ViT and RNN** As shown above, for AnyNet, the input spectrogram is processed as a image and fed in the classifier; for ViT, the input is separated as several patches for the attention processing; for RNN, the input is cut as temporal slices and given to the classifier sequentially.

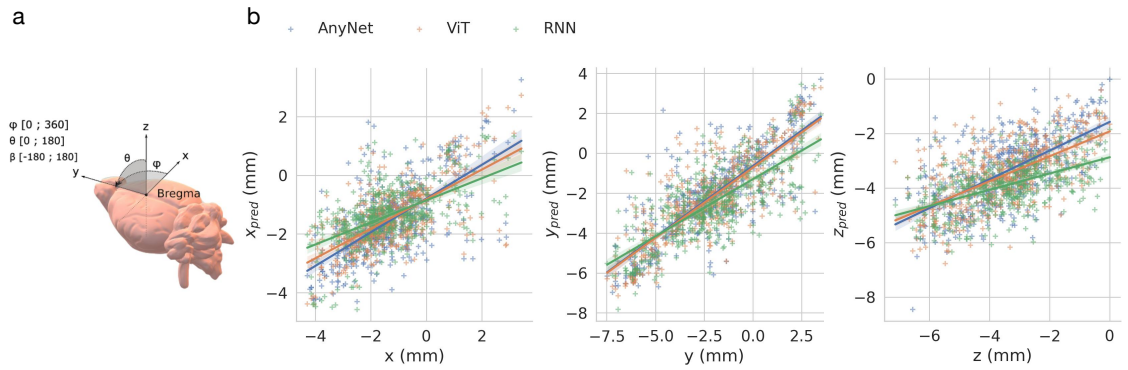

Supplementary Figure 2: **Deep learning-based regression for stereotactic coordinates using LFPs. a.** Illustration of stereotactic coordinates in mouse brain. **b.** Regression for x, y and z axis using LFPs. Deep learning methods, AnyNet, ViT, and RNN are able to predict stereotactic coordinates. For x axis, AnyNet ($R^2 = 0.356, r = 0.656, p < 0.001$), ViT ($R^2 = 0.433, r = 0.672, p < 0.001$), and RNN ($R^2 = 0.2889, r = 0.553, p < 0.001$). For y axis, AnyNet ($R^2 = 0.655, r = 0.812, p < 0.001$), ViT ($R^2 = 0.683, r = 0.828, p < 0.001$), and RNN ($R^2 = 0.527, r = 0.746, p < 0.001$). For z axis, AnyNet ($R^2 = 0.395, r = 0.650, p < 0.001$), ViT ($R^2 = 0.373, r = 0.622, p < 0.001$), RNN ($R^2 = 0.197, r = 0.534, p < 0.001$)

.

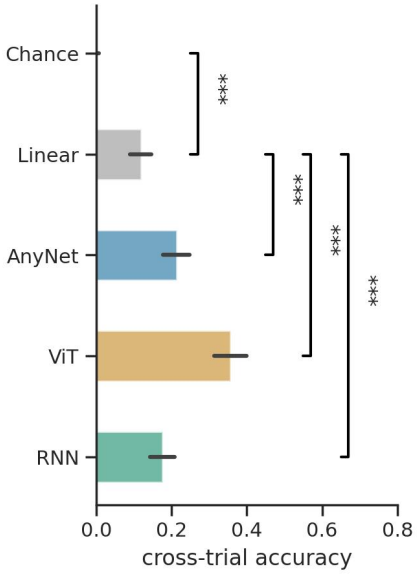

Supplementary Figure 3: **Classification using mean spectrogram of inter-trial state.** Overall cross-trial accuracy from distinct classifiers: linear network model, AnyNet, ViT, and RNN. Linear classifier performs significantly better than the chance level ($p < 0.001$). The three deep networks (AnyNet, ViT, and RNN) outperform the linear classifier ($p < 0.001$). Overall cross-trial accuracy: linear model (0.119), AnyNet (0.213), ViT(0.357), and RNN (0.176).

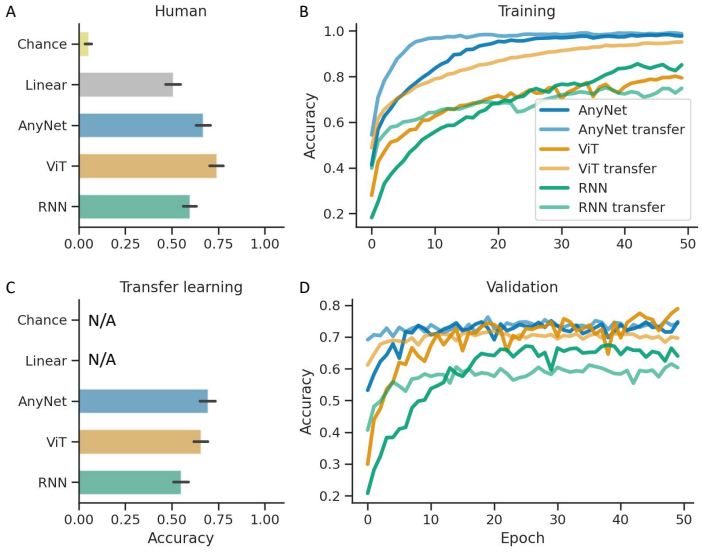

Supplementary Figure 4: **Pre-training on mouse data accelerates training on human data.** **a.** Overall cross-trial accuracy for the human Neuropixels dataset trained from random initialization. **b.** Training accuracy of three classifiers for the transfer learning and training from the random initialization. **c.** Cross-trial accuracy for the transfer learning of three classifiers. **d.** Validation accuracy curves during training for three classifiers during transfer learning.

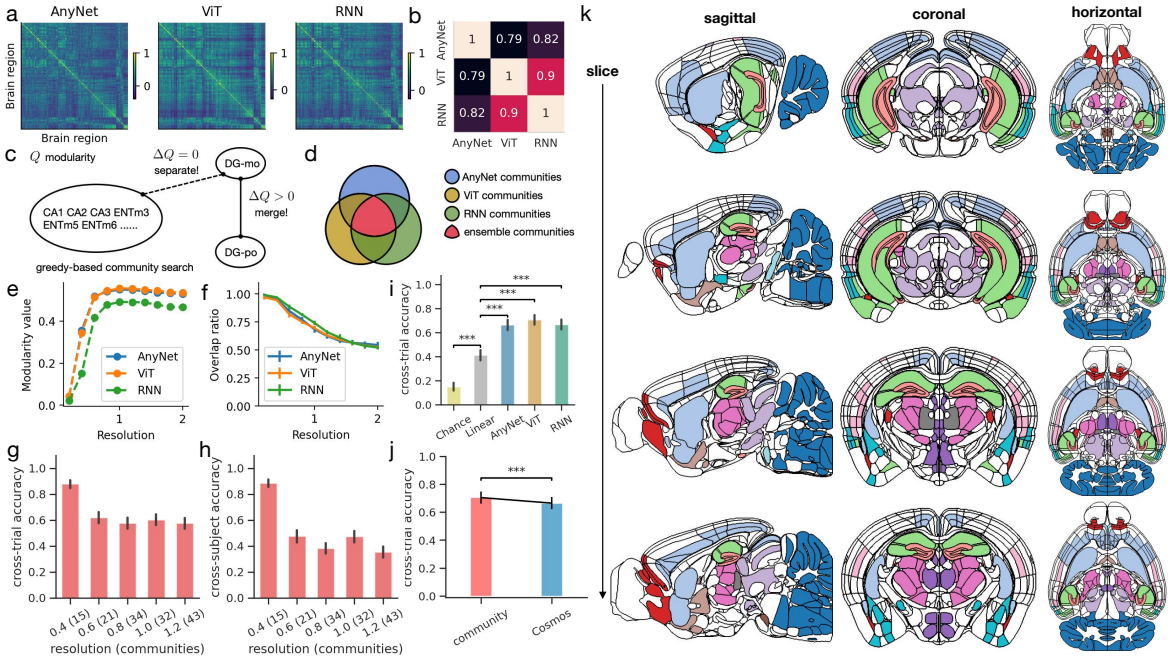

Supplementary Figure 5: **Spectral similarities define communities a**. Heat map showing the correlation coefficient of the classifier's penultimate layer activations of one Allen brain atlas area to another. Ordering follows Fig. 2c. **b**. Similarity analysis for the correlation matrices of the three different models, each square shows the correlation coefficient between the matrices shown in a. **c**. Schematics of greedy modularity search for communities in 472 brain regions. If merging two separated communities increases overall modularity, then a new community is generated; otherwise, those two communities remain isolated modules. **d**. Schematic for establishing a consensus across ANNs. Ensemble communities are obtained by first aligning each community across ANNs and then only keeping the brain areas that were found to belong to that community consistently across the three ANNs. **e**. Final modularity values of greedy search is shown for different resolutions. **f.** The overlap ratio between communities found using all brain areas and communities using 80 % of the brain areas. **g**. Average cross-trial accuracy for ensemble communities at different resolutions, the number of communities is shown in parentheses. **h**. Same as g but for cross-trial accuracy. **i**. Overall cross-trial accuracy for the different algorithms trained to classify the 10-region anatomical atlas 'Cosmos'. **j**. Comparing community with Cosmos at a matched number of 10 classes in terms of the cross-trial accuracy. **k**. Sagittal, coronal and horizontal slices showing 18 ensemble communities out of the 32 using different colors. Only 18 are shown for enhanced visualization, hence the white areas are either areas that did not belong to any community, or areas that were in the 14 communities that could not be shown simultaneously.

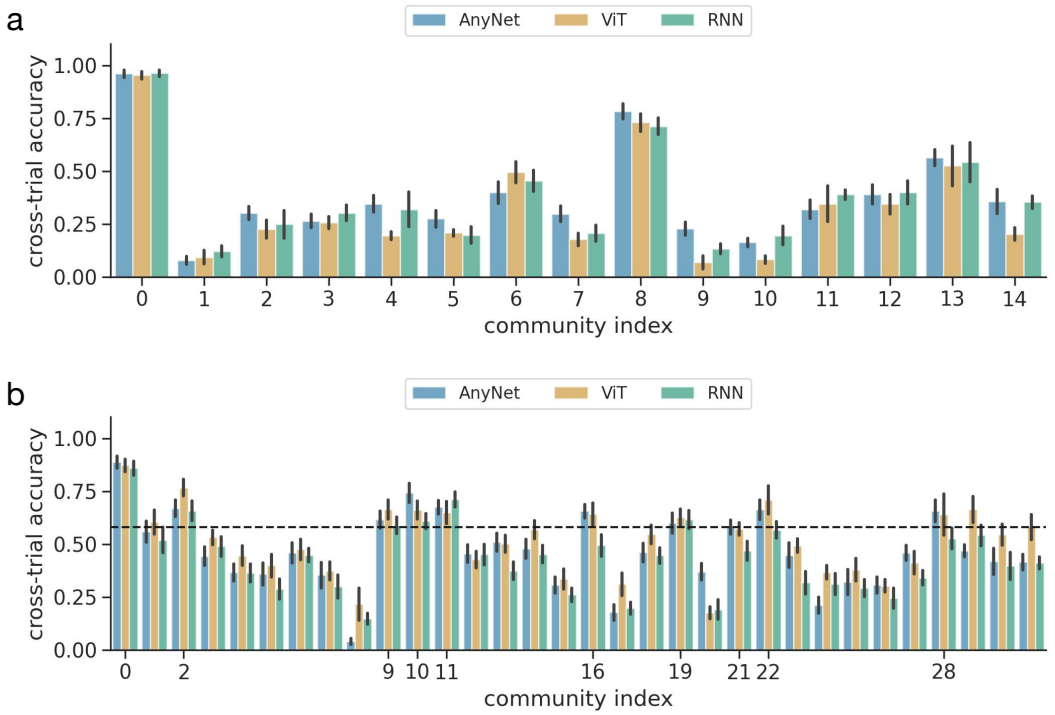

Supplementary Figure 6: **Individual cross-trial accuracy for communities under different resolutions. a.** Individual cross-trial accuracy for communities under 0.4 resolutions. **b.** Individual cross-trial accuracy for communities under 1.0 resolutions. Communities which individual accuracy for AnyNet are in Top 10 (above the dash line) are selected as landmark communities.

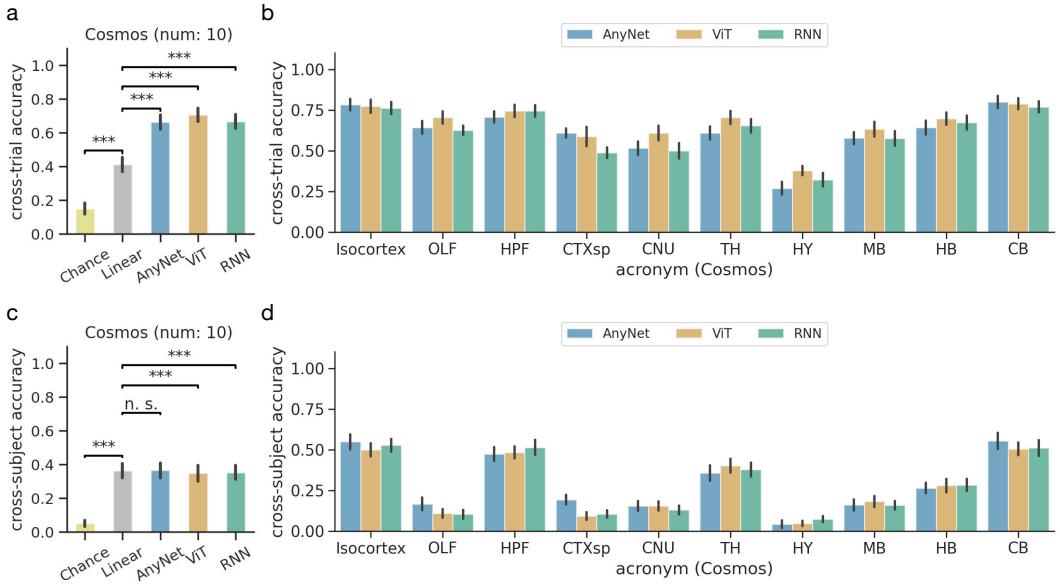

Supplementary Figure 7: **Classification of Cosmos mapping. a.** Overall cross-trial accuracy for Cosmos mapping. **b.** Individual cross-trial accuracy for Cosmos mapping. **c.** Overall cross-subject accuracy for Cosmos mapping. **d.** Individual cross-subject accuracy for Cosmos mapping.

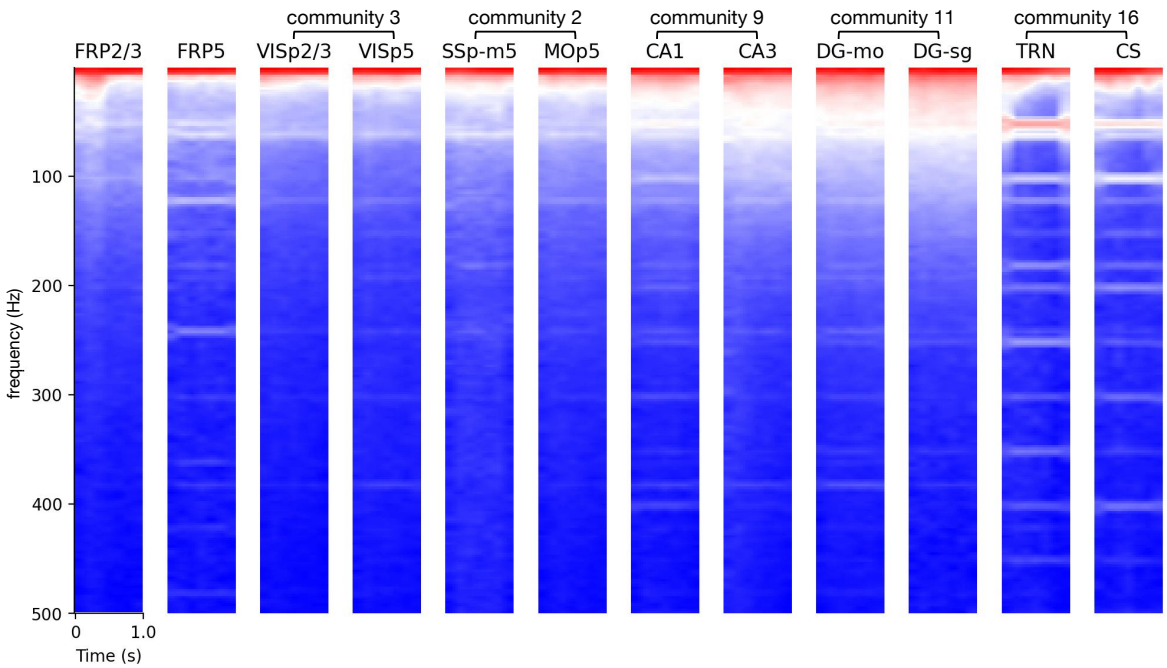

Supplementary Figure 8: **Mean spectrogram of distinct brain areas of inter-trial state.** Power spectra were normalized and read out with a logarithm for visualization. Red means high amplitude; and blue represents low amplitude. Brain areas from the same community are marked. Much of the bar structure seen in, for instance, TRN arises from scaling a lower power signal that contained the alternative current artifact (at 50 Hz for European labs and 60 Hz for American labs) and its harmonics.

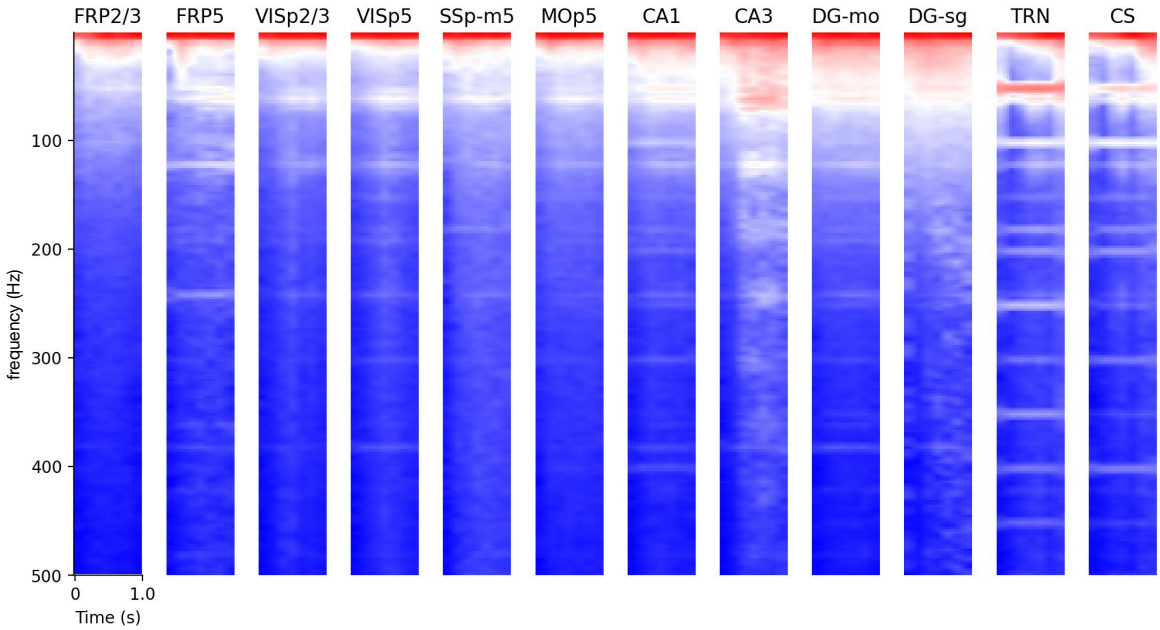

Supplementary Figure 9: **Mean spectrogram of distinct brain areas of task period.** Same as Supplementary Fig. 8 we show the logarithm of the mean spectrogram of task period.

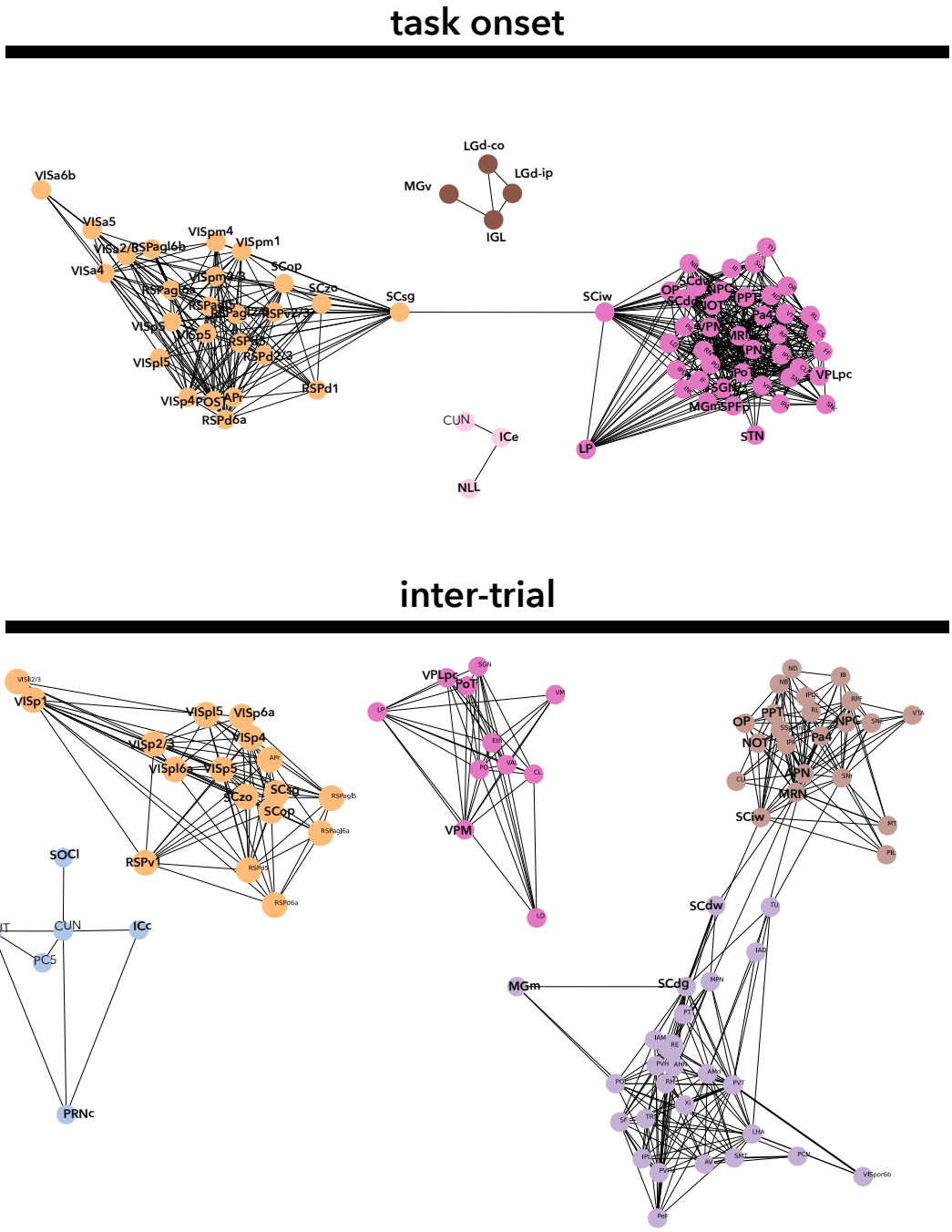

Supplementary Figure 10: **Electrospectral for basic audio-visual areas.** Selection of communities containing areas associated with lower order subcortical visual sensory (lateral geniculate nucleus, LGd, superior colliculus, SCop, SCzo and SCsg), auditory (inferior colliculus ICc, medial geniculate nucleus, MGm, MGv, Nucleus of the Lateral Lemniscus NLL, superior olive SOCl), oculomotor (MRN, APN, Pa4, NOT, IP, PPT, superior colliculus, SCiw, SCdw and SCdg) and auditory reflexes (caudal part of pontine reticular nucleus PRNc) information. Graph links represent thresholded confusion matrix element with line thickness.

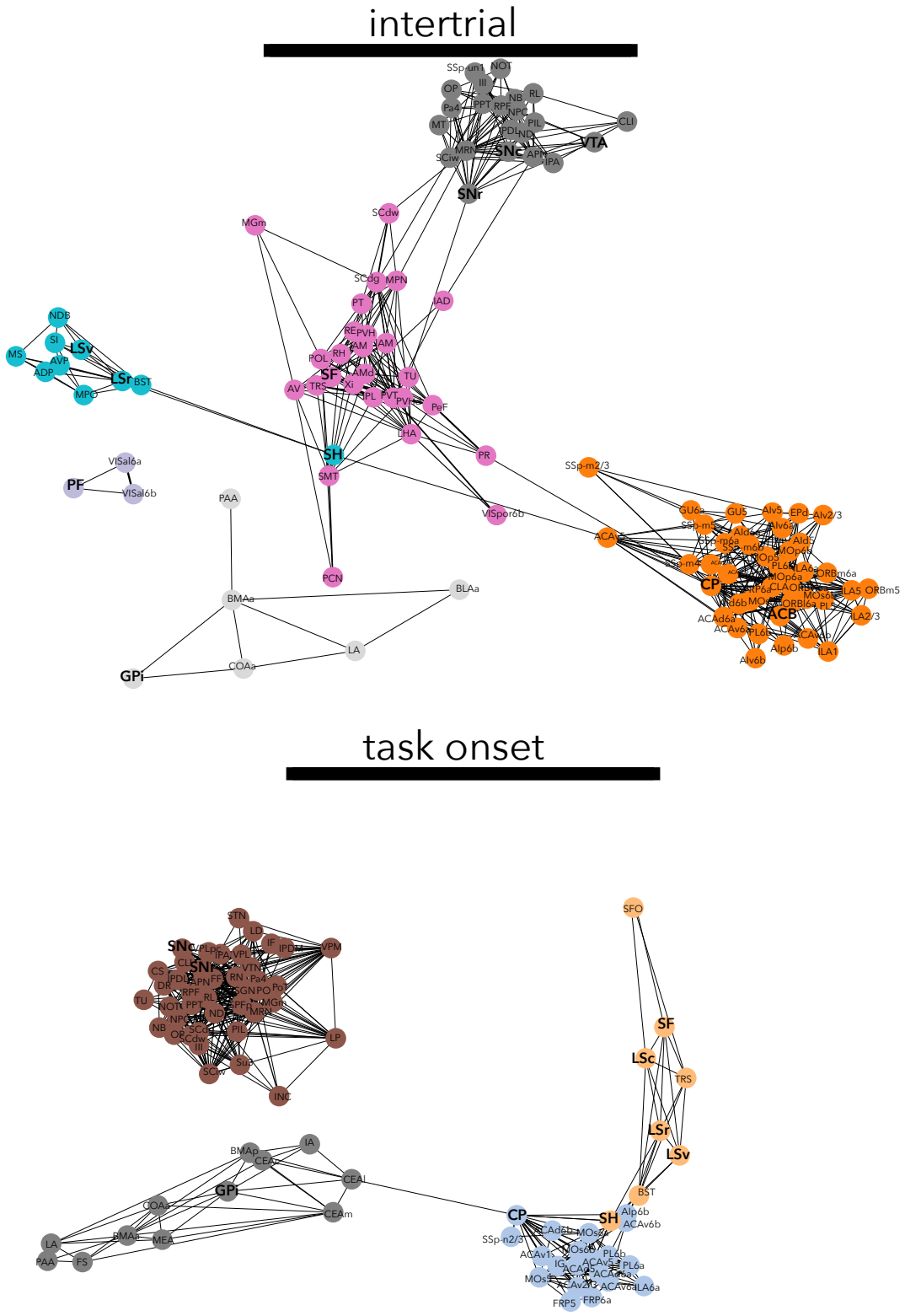

Supplementary Figure 11: **Electrospectral for kinematics system.** Selection of communities containing areas associated with kinematics: putamen (CP), parafasacicular nucleus (PF), lateral septum (LSr, LSv), globus pallidus (GPi), nucleus accumbens (ACB), septofimbrial nucleus (SF), septohippocampal nucleus (SN), Substantia Nigra (SNr, SNc).

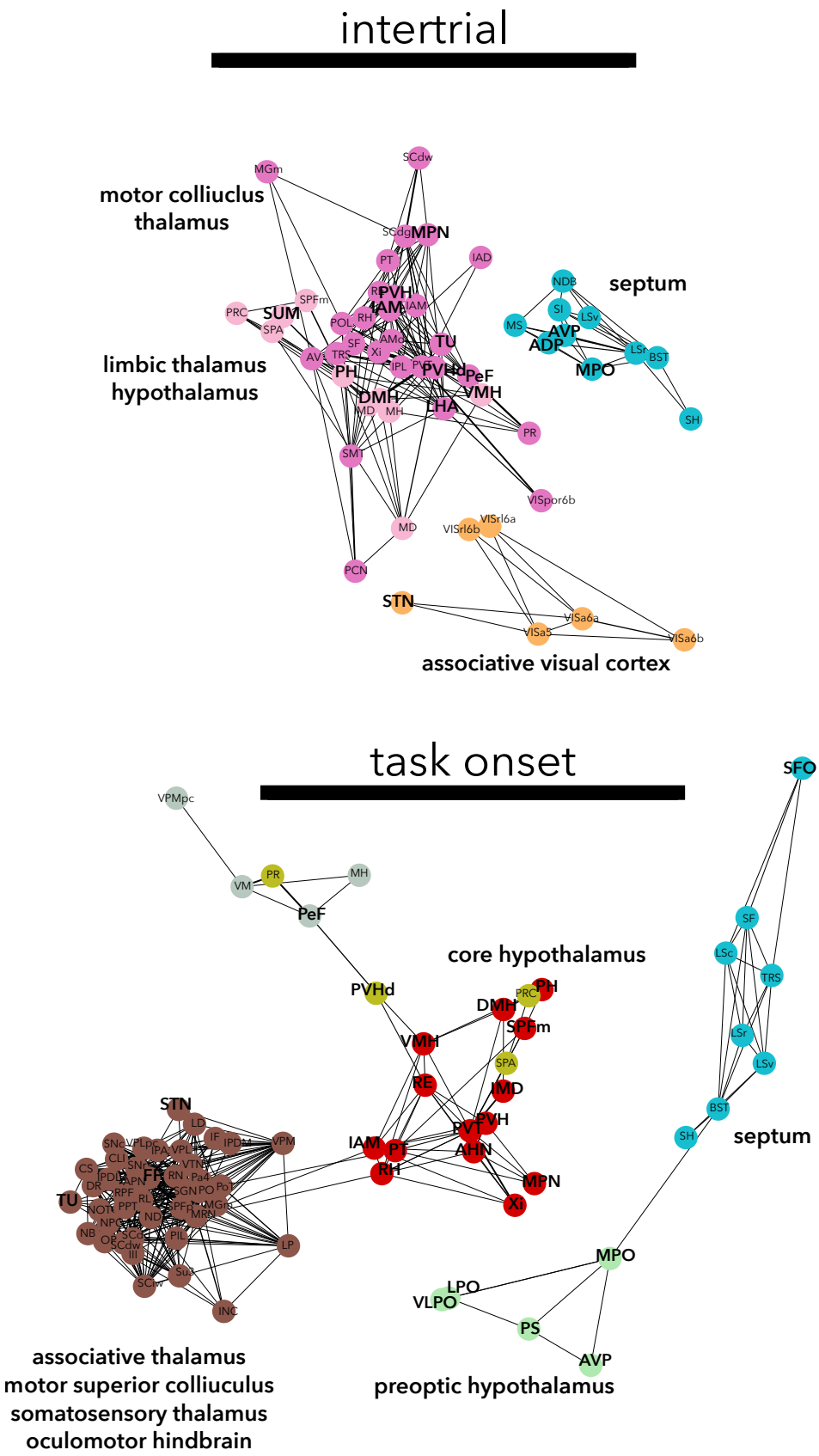

Supplementary Figure 12: **Electrospectral for the hypothalamus.** Selection of communities containing areas that belong to the hypothalamus.

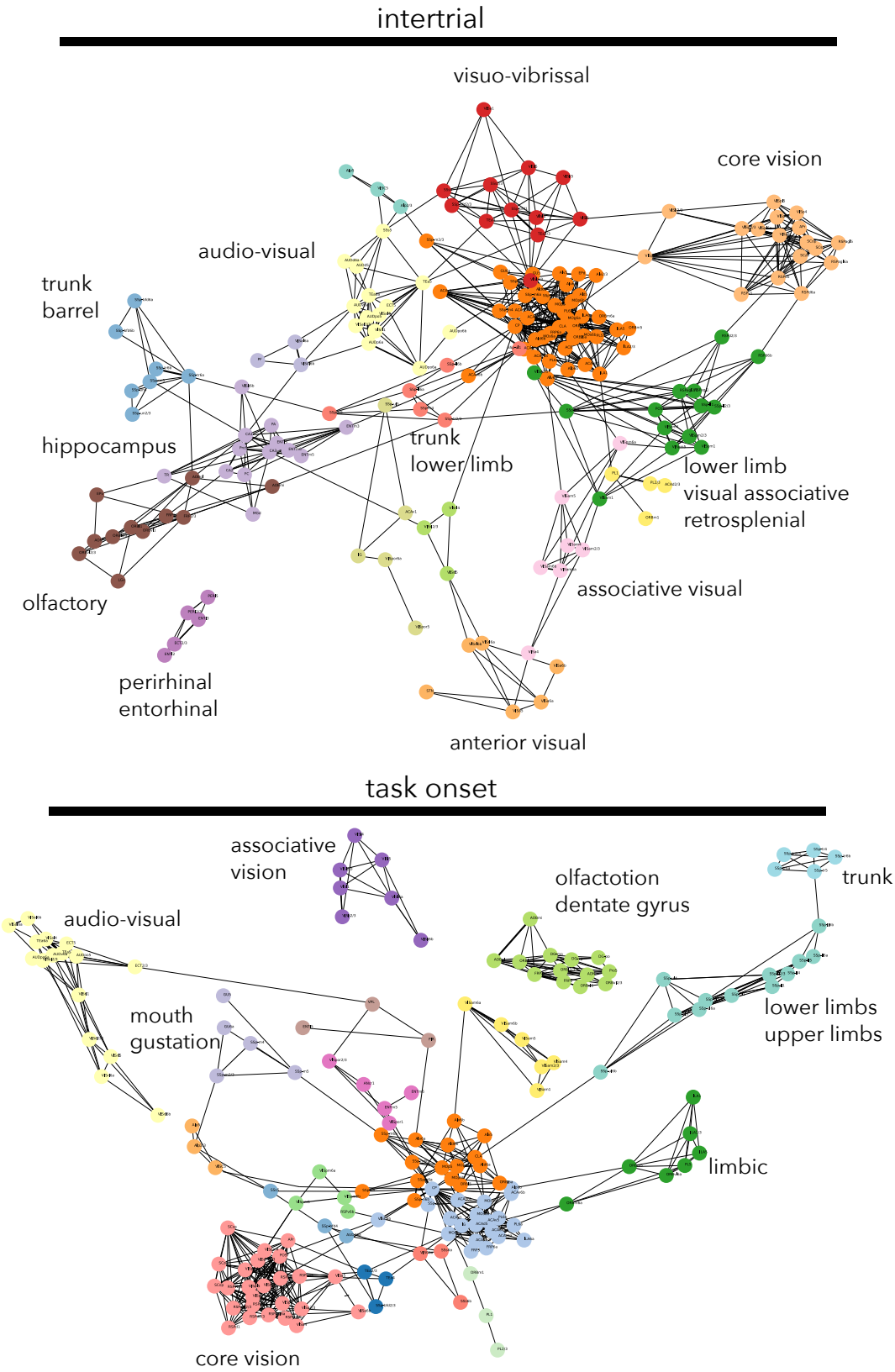

Supplementary Figure 13: **Electrospectral communities for cortical areas.** Selection of communities containing areas that belong to the isocortex.

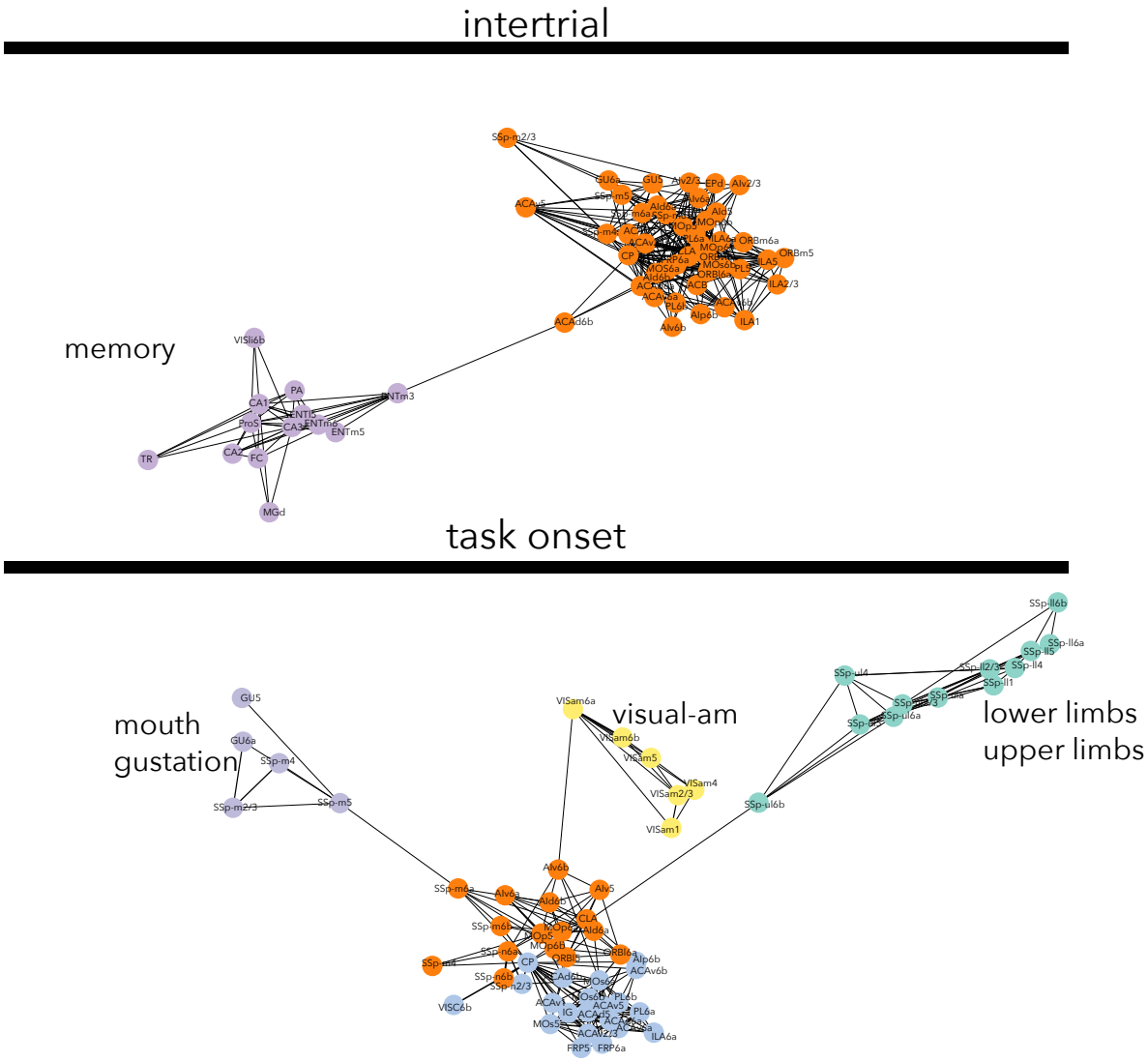

Supplementary Figure 14: **Selection intercommunity links with single connector nodes.** Top: for intertrial communities, the memory community links to the motor planning community through layer 3 of the medial entorhinal cortex (ENTm3) and layer 6b of the anterior cingulate area (ACA6b). Bottom, for the task communities linking to the two motor planning communities, the gustatory community hinges on the layer 5 and 6 of mouth somatosensory cortex, visual-am through layer 6 of anteromedial visual cortex and agranular insular cortex layer 6b. The limbs community links through putamen and somatosensory upper limb layer 6b.

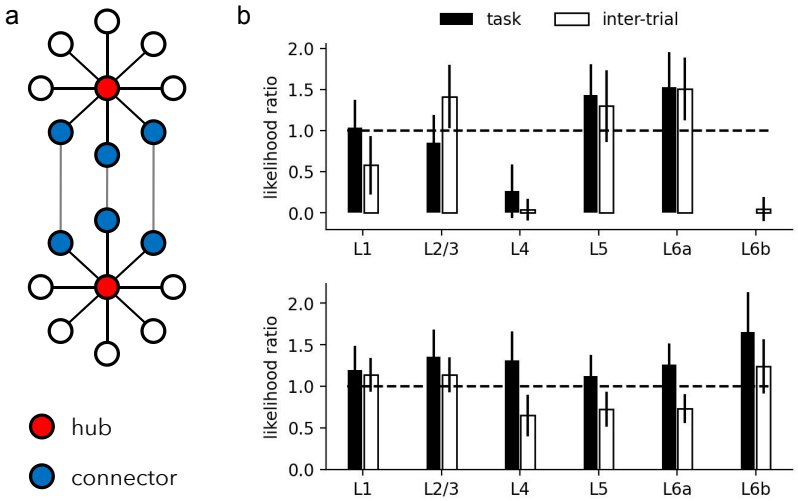

Supplementary Figure 15: **Layer specificity of hub and connector nodes. a** Schematic definition of hub and connector nodes. **b** The ratio of probability (likelihood ratio) is defined as the bootstrapping estimate of the probability that a layer is attributed as a hub divided by the bootstrapping estimate of the probability that a layer is attributed to any community. **c** The likelihood ratio for a given layer to be a connector node. Errorbars represent standard deviation over 30 subsampled confusion matrices (Methods; Graph Theory Methods

Supplementary Table 1: Table for community labels of each area.

Allen acronym	**Allen name**	**Cosmos acronym**	**Cosmos name**	**Inter-trial**	**Audio-visual cue**
FRP1	Frontal pole layer 1	Isocortex	Isocortex	10	26
FRP2/3	Frontal pole layer 2/3	Isocortex	Isocortex	10	26
FRP5	Frontal pole layer 5	Isocortex	Isocortex	-1	1
FRP6a	Frontal pole layer 6a	Isocortex	Isocortex	2	1
MOp1	Primary motor area Layer 1	Isocortex	Isocortex	-1	-1
MOp2/3	Primary motor area Layer 2/3	Isocortex	Isocortex	-1	-1
MOp5	Primary motor area Layer 5	Isocortex	Isocortex	2	2
MOp6a	Primary motor area Layer 6a	Isocortex	Isocortex	2	2
MOp6b	Primary motor area Layer 6b	Isocortex	Isocortex	2	2
MOs1	Secondary motor area layer 1	Isocortex	Isocortex	-1	-1
MOs2/3	Secondary motor area layer 2/3	Isocortex	Isocortex	-1	-1
MOs5	Secondary motor area layer 5	Isocortex	Isocortex	-1	1
MOs6a	Secondary motor area layer 6a	Isocortex	Isocortex	2	1
MOs6b	Secondary motor area layer 6b	Isocortex	Isocortex	2	1
SSp-n1	Primary somatosensory area nose layer 1	Isocortex	Isocortex	-1	-1
SSp-n2/3	Primary somatosensory area nose layer 2/3	Isocortex	Isocortex	-1	1
SSp-n4	Primary somatosensory area nose layer 4	Isocortex	Isocortex	-1	2
SSp-n5	Primary somatosensory area nose layer 5	Isocortex	Isocortex	-1	-1
SSp-n6a	Primary somatosensory area nose layer 6a	Isocortex	Isocortex	-1	2
SSp-n6b	Primary somatosensory area nose layer 6b	Isocortex	Isocortex	-1	2
SSp-bfd1	Primary somatosensory area barrel field layer 1	Isocortex	Isocortex	6	-1
SSp-bfd2/3	Primary somatosensory area barrel field layer 2/3	Isocortex	Isocortex	6	0
SSp-bfd4	Primary somatosensory area barrel field layer 4	Isocortex	Isocortex	5	24
SSp-bfd5	Primary somatosensory area barrel field layer 5	Isocortex	Isocortex	5	-1
SSp-bfd6a	Primary somatosensory area barrel field layer 6a	Isocortex	Isocortex	24	-1
SSp-bfd6b	Primary somatosensory area barrel field layer 6b	Isocortex	Isocortex	24	-1
SSp-ll1	Primary somatosensory area lower limb layer 1	Isocortex	Isocortex	4	20
SSp-ll2/3	Primary somatosensory area lower limb layer 2/3	Isocortex	Isocortex	4	20
SSp-ll4	Primary somatosensory area lower limb layer 4	Isocortex	Isocortex	-1	20
SSp-ll5	Primary somatosensory area lower limb layer 5	Isocortex	Isocortex	-1	20
SSp-ll6a	Primary somatosensory area lower limb layer 6a	Isocortex	Isocortex	23	20

Allen acronym	Allen name	Cosmos acronym	Cosmos name	Inter-trial	Audio-visual cue
SSp-ll6b	Primary somatosensory area lower limb layer 6b	Isocortex	Isocortex	23	20
SSp-m1	Primary somatosensory area mouth layer 1	Isocortex	Isocortex	-1	-1
SSp-m2/3	Primary somatosensory area mouth layer 2/3	Isocortex	Isocortex	2	22
SSp-m4	Primary somatosensory area mouth layer 4	Isocortex	Isocortex	2	22
SSp-m5	Primary somatosensory area mouth layer 5	Isocortex	Isocortex	2	22
SSp-m6a	Primary somatosensory area mouth layer 6a	Isocortex	Isocortex	2	2
SSp-m6b	Primary somatosensory area mouth layer 6b	Isocortex	Isocortex	2	2
SSp-ul1	Primary somatosensory area upper limb layer 1	Isocortex	Isocortex	23	20
SSp-ul2/3	Primary somatosensory area upper limb layer 2/3	Isocortex	Isocortex	-1	20
SSp-ul4	Primary somatosensory area upper limb layer 4	Isocortex	Isocortex	-1	20
SSp-ul5	Primary somatosensory area upper limb layer 5	Isocortex	Isocortex	17	20
SSp-ul6a	Primary somatosensory area upper limb layer 6a	Isocortex	Isocortex	-1	20
SSp-ul6b	Primary somatosensory area upper limb layer 6b	Isocortex	Isocortex	-1	20
SSp-tr1	Primary somatosensory area trunk layer 1	Isocortex	Isocortex	4	-1
SSp-tr2/3	Primary somatosensory area trunk layer 2/3	Isocortex	Isocortex	23	19
SSp-tr4	Primary somatosensory area trunk layer 4	Isocortex	Isocortex	23	19
SSp-tr5	Primary somatosensory area trunk layer 5	Isocortex	Isocortex	23	19
SSp-tr6a	Primary somatosensory area trunk layer 6a	Isocortex	Isocortex	24	19
SSp-tr6b	Primary somatosensory area trunk layer 6b	Isocortex	Isocortex	24	19
SSp-un1	Primary somatosensory area unassigned layer 1	Isocortex	Isocortex	14	-1
SSp-un2/3	Primary somatosensory area unassigned layer 2/3	Isocortex	Isocortex	24	-1
SSp-un4	Primary somatosensory area unassigned layer 4	Isocortex	Isocortex	24	-1
SSp-un5	Primary somatosensory area unassigned layer 5	Isocortex	Isocortex	24	-1
SSp-un6a	Primary somatosensory area unassigned layer 6a	Isocortex	Isocortex	-1	-1
SSp-un6b	Primary somatosensory area unassigned layer 6b	Isocortex	Isocortex	-1	-1
SSs2/3	Supplemental somatosensory area layer 2/3	Isocortex	Isocortex	6	6

Allen acronym	Allen name	Cosmos acronym	Cosmos name	Inter-trial	Audio-visual cue
SSs4	Supplemental somatosensory area layer 4	Isocortex	Isocortex	6	-1
SSs5	Supplemental somatosensory area layer 5	Isocortex	Isocortex	21	24
SSs6a	Supplemental somatosensory area layer 6a	Isocortex	Isocortex	-1	23
SSs6b	Supplemental somatosensory area layer 6b	Isocortex	Isocortex	-1	23
GU5	Gustatory areas layer 5	Isocortex	Isocortex	2	22
GU6a	Gustatory areas layer 6a	Isocortex	Isocortex	2	22
VISC5	Visceral area layer 5	Isocortex	Isocortex	20	25
VISC6a	Visceral area layer 6a	Isocortex	Isocortex	-1	23
VISC6b	Visceral area layer 6b	Isocortex	Isocortex	-1	1
AUDd2/3	Dorsal auditory area layer 2/3	Isocortex	Isocortex	-1	-1
AUDd4	Dorsal auditory area layer 4	Isocortex	Isocortex	-1	-1
AUDd5	Dorsal auditory area layer 5	Isocortex	Isocortex	21	-1
AUDd6a	Dorsal auditory area layer 6a	Isocortex	Isocortex	21	24
AUDd6b	Dorsal auditory area layer 6b	Isocortex	Isocortex	-1	-1
AUDp4	Primary auditory area layer 4	Isocortex	Isocortex	-1	-1
AUDp5	Primary auditory area layer 5	Isocortex	Isocortex	-1	-1
AUDp6a	Primary auditory area layer 6a	Isocortex	Isocortex	21	-1
AUDpo2/3	Posterior auditory area layer 2/3	Isocortex	Isocortex	-1	-1
AUDpo4	Posterior auditory area layer 4	Isocortex	Isocortex	-1	-1
AUDpo5	Posterior auditory area layer 5	Isocortex	Isocortex	21	21
AUDpo6a	Posterior auditory area layer 6a	Isocortex	Isocortex	21	21
AUDpo6b	Posterior auditory area layer 6b	Isocortex	Isocortex	21	-1
AUDv5	Ventral auditory area layer 5	Isocortex	Isocortex	-1	-1
AUDv6a	Ventral auditory area layer 6a	Isocortex	Isocortex	21	21
AUDv6b	Ventral auditory area layer 6b	Isocortex	Isocortex	-1	-1
VISal2/3	Anterolateral visual area layer 2/3	Isocortex	Isocortex	21	21
VISal4	Anterolateral visual area layer 4	Isocortex	Isocortex	21	21
VISal5	Anterolateral visual area layer 5	Isocortex	Isocortex	-1	-1
VISal6a	Anterolateral visual area layer 6a	Isocortex	Isocortex	22	21
VISal6b	Anterolateral visual area layer 6b	Isocortex	Isocortex	22	21
VISam1	Anteromedial visual area layer 1	Isocortex	Isocortex	4	31
VISam2/3	Anteromedial visual area layer 2/3	Isocortex	Isocortex	27	31
VISam4	Anteromedial visual area layer 4	Isocortex	Isocortex	27	31
VISam5	Anteromedial visual area layer 5	Isocortex	Isocortex	27	31
VISam6a	Anteromedial visual area layer 6a	Isocortex	Isocortex	27	31
VISam6b	Anteromedial visual area layer 6b	Isocortex	Isocortex	27	31
VISl1	Lateral visual area layer 1	Isocortex	Isocortex	6	8
VISl2/3	Lateral visual area layer 2/3	Isocortex	Isocortex	6	8
VISl4	Lateral visual area layer 4	Isocortex	Isocortex	6	8
VISl5	Lateral visual area layer 5	Isocortex	Isocortex	6	8
VISl6a	Lateral visual area layer 6a	Isocortex	Isocortex	-1	8
VISl6b	Lateral visual area layer 6b	Isocortex	Isocortex	-1	-1
VISp1	Primary visual area layer 1	Isocortex	Isocortex	3	7
VISp2/3	Primary visual area layer 2/3	Isocortex	Isocortex	3	6
VISp4	Primary visual area layer 4	Isocortex	Isocortex	3	7
VISp5	Primary visual area layer 5	Isocortex	Isocortex	3	7
VISp6a	Primary visual area layer 6a	Isocortex	Isocortex	3	-1
VISp6b	Primary visual area layer 6b	Isocortex	Isocortex	-1	-1
VISpl1	Posterolateral visual area layer 1	Isocortex	Isocortex	5	-1

Allen acronym	Allen name	Cosmos acronym	Cosmos name	Inter-trial	Audio-visual cue
VISpl2/3	Posterolateral visual area layer 2/3	Isocortex	Isocortex	-1	-1
VISpl4	Posterolateral visual area layer 4	Isocortex	Isocortex	-1	-1
VISpl5	Posterolateral visual area layer 5	Isocortex	Isocortex	3	7
VISpl6a	Posterolateral visual area layer 6a	Isocortex	Isocortex	3	6
VISpm1	posteromedial visual area layer 1	Isocortex	Isocortex	4	7
VISpm2/3	posteromedial visual area layer 2/3	Isocortex	Isocortex	4	7
VISpm4	posteromedial visual area layer 4	Isocortex	Isocortex	4	7
VISpm5	posteromedial visual area layer 5	Isocortex	Isocortex	4	5
VISpm6a	posteromedial visual area layer 6a	Isocortex	Isocortex	27	5
VISpm6b	posteromedial visual area layer 6b	Isocortex	Isocortex	-1	5
VISli2/3	Laterointermediate area layer 2/3	Isocortex	Isocortex	3	8
VISli4	Laterointermediate area layer 4	Isocortex	Isocortex	-1	-1
VISli5	Laterointermediate area layer 5	Isocortex	Isocortex	6	-1
VISli6a	Laterointermediate area layer 6a	Isocortex	Isocortex	8	-1
VISli6b	Laterointermediate area layer 6b	Isocortex	Isocortex	9	8
VISpor1	Postrhinal area layer 1	Isocortex	Isocortex	-1	12
VISpor2/3	Postrhinal area layer 2/3	Isocortex	Isocortex	-1	12
VISpor5	Postrhinal area layer 5	Isocortex	Isocortex	17	-1
VISpor6a	Postrhinal area layer 6a	Isocortex	Isocortex	17	-1
VISpor6b	Postrhinal area layer 6b	Isocortex	Isocortex	12	-1
ACAd2/3	Anterior cingulate area dorsal part layer 2/3	Isocortex	Isocortex	31	-1
ACAd5	Anterior cingulate area dorsal part layer 5	Isocortex	Isocortex	2	1
ACAd6a	Anterior cingulate area dorsal part layer 6a	Isocortex	Isocortex	2	1
ACAd6b	Anterior cingulate area dorsal part layer 6b	Isocortex	Isocortex	2	1
ACAv1	Anterior cingulate area ventral part layer 1	Isocortex	Isocortex	17	1
ACAv2/3	Anterior cingulate area ventral part layer 2/3	Isocortex	Isocortex	2	1
ACAv5	Anterior cingulate area ventral part layer 5	Isocortex	Isocortex	2	1
ACAv6a	Anterior cingulate area ventral part 6a	Isocortex	Isocortex	2	1
ACAv6b	Anterior cingulate area ventral part 6b	Isocortex	Isocortex	2	1
PL1	Prelimbic area layer 1	Isocortex	Isocortex	31	30
PL2/3	Prelimbic area layer 2/3	Isocortex	Isocortex	31	30
PL5	Prelimbic area layer 5	Isocortex	Isocortex	2	4
PL6a	Prelimbic area layer 6a	Isocortex	Isocortex	2	1
PL6b	Prelimbic area layer 6b	Isocortex	Isocortex	2	1
ILA1	Infralimbic area layer 1	Isocortex	Isocortex	2	4
ILA2/3	Infralimbic area layer 2/3	Isocortex	Isocortex	2	4
ILA5	Infralimbic area layer 5	Isocortex	Isocortex	2	4
ILA6a	Infralimbic area layer 6a	Isocortex	Isocortex	2	1
ORBl1	Orbital area lateral part layer 1	Isocortex	Isocortex	10	26
ORBl2/3	Orbital area lateral part layer 2/3	Isocortex	Isocortex	10	26
ORBl5	Orbital area lateral part layer 5	Isocortex	Isocortex	7	2
ORBl6a	Orbital area lateral part layer 6a	Isocortex	Isocortex	2	2
ORBm1	Orbital area medial part layer 1	Isocortex	Isocortex	31	30
ORBm2/3	Orbital area medial part layer 2/3	Isocortex	Isocortex	7	-1

Allen acronym	Allen name	Cosmos acronym	Cosmos name	Inter-trial	Audio-visual cue
ORBm5	Orbital area medial part layer 5	Isocortex	Isocortex	2	4
ORBm6a	Orbital area medial part layer 6a	Isocortex	Isocortex	2	4
ORBvl1	Orbital area ventrolateral part layer 1	Isocortex	Isocortex	10	26
ORBvl2/3	Orbital area ventrolateral part layer 2/3	Isocortex	Isocortex	10	26
ORBvl5	Orbital area ventrolateral part layer 5	Isocortex	Isocortex	-1	-1
ORBvl6a	Orbital area ventrolateral part layer 6a	Isocortex	Isocortex	2	4
AId5	Agranular insular area dorsal part layer 5	Isocortex	Isocortex	2	-1
AId6a	Agranular insular area dorsal part layer 6a	Isocortex	Isocortex	2	2
AId6b	Agranular insular area dorsal part layer 6b	Isocortex	Isocortex	2	2
AIp1	Agranular insular area posterior part layer 1	Isocortex	Isocortex	-1	23
AIp2/3	Agranular insular area posterior part layer 2/3	Isocortex	Isocortex	20	25
AIp5	Agranular insular area posterior part layer 5	Isocortex	Isocortex	20	25
AIp6a	Agranular insular area posterior part layer 6a	Isocortex	Isocortex	-1	-1
AIp6b	Agranular insular area posterior part layer 6b	Isocortex	Isocortex	2	1
AIv2/3	Agranular insular area ventral part layer 2/3	Isocortex	Isocortex	2	-1
AIv5	Agranular insular area ventral part layer 5	Isocortex	Isocortex	2	2
AIv6a	Agranular insular area ventral part layer 6a	Isocortex	Isocortex	2	2
AIv6b	Agranular insular area ventral part layer 6b	Isocortex	Isocortex	2	2
RSPagl1	Retrosplenial area lateral agranular part layer 1	Isocortex	Isocortex	4	-1
RSPagl2/3	Retrosplenial area lateral agranular part layer 2/3	Isocortex	Isocortex	4	7
RSPagl5	Retrosplenial area lateral agranular part layer 5	Isocortex	Isocortex	3	7
RSPagl6a	Retrosplenial area lateral agranular part layer 6a	Isocortex	Isocortex	3	7
RSPagl6b	Retrosplenial area lateral agranular part layer 6b	Isocortex	Isocortex	-1	7
RSPd1	Retrosplenial area dorsal part layer 1	Isocortex	Isocortex	-1	7
RSPd2/3	Retrosplenial area dorsal part layer 2/3	Isocortex	Isocortex	4	7
RSPd5	Retrosplenial area dorsal part layer 5	Isocortex	Isocortex	3	7
RSPd6a	Retrosplenial area dorsal part layer 6a	Isocortex	Isocortex	3	7

Allen acronym	Allen name	Cosmos acronym	Cosmos name	Inter-trial	Audio-visual cue
RSPd6b	Retrosplenial area dorsal part layer 6b	Isocortex	Isocortex	4	5
RSPv1	Retrosplenial area ventral part layer 1	Isocortex	Isocortex	3	-1
RSPv2/3	Retrosplenial area ventral part layer 2/3	Isocortex	Isocortex	-1	7
RSPv5	Retrosplenial area ventral part layer 5	Isocortex	Isocortex	-1	-1
RSPv6a	Retrosplenial area ventral part layer 6a	Isocortex	Isocortex	-1	6
RSPv6b	Retrosplenial area ventral part layer 6b	Isocortex	Isocortex	-1	5
VISa1	Anterior area layer 1	Isocortex	Isocortex	6	-1
VISa2/3	Anterior area layer 2/3	Isocortex	Isocortex	4	7
VISa4	Anterior area layer 4	Isocortex	Isocortex	27	7
VISa5	Anterior area layer 5	Isocortex	Isocortex	25	7
VISa6a	Anterior area layer 6a	Isocortex	Isocortex	25	-1
VISa6b	Anterior area layer 6b	Isocortex	Isocortex	25	7
VISrl1	Rostrolateral area layer 1	Isocortex	Isocortex	21	21
VISrl2/3	Rostrolateral area layer 2/3	Isocortex	Isocortex	26	21
VISrl4	Rostrolateral area layer 4	Isocortex	Isocortex	26	-1
VISrl5	Rostrolateral area layer 5	Isocortex	Isocortex	26	21
VISrl6a	Rostrolateral area layer 6a	Isocortex	Isocortex	25	21
VISrl6b	Rostrolateral area layer 6b	Isocortex	Isocortex	25	21
TEa2/3	Temporal association areas layer 2/3	Isocortex	Isocortex	6	0
TEa4	Temporal association areas layer 4	Isocortex	Isocortex	6	0
TEa5	Temporal association areas layer 5	Isocortex	Isocortex	21	21
TEa6a	Temporal association areas layer 6a	Isocortex	Isocortex	21	21
TEa6b	Temporal association areas layer 6b	Isocortex	Isocortex	8	-1
PERI1	Perirhinal area layer 1	Isocortex	Isocortex	-1	-1
PERI2/3	Perirhinal area layer 2/3	Isocortex	Isocortex	29	-1
PERI5	Perirhinal area layer 5	Isocortex	Isocortex	29	-1
ECT2/3	Ectorhinal area/Layer 2/3	Isocortex	Isocortex	29	21
ECT5	Ectorhinal area/Layer 5	Isocortex	Isocortex	21	21
ECT6a	Ectorhinal area/Layer 6a	Isocortex	Isocortex	-1	-1
ECT6b	Ectorhinal area/Layer 6b	Isocortex	Isocortex	-1	-1
AOBgl	Accessory olfactory bulb glomerular layer	OLF	Olfactory areas	10	26
AOBmi	Accessory olfactory bulb mitral layer	OLF	Olfactory areas	10	26
DG-mo	Dentate gyrus molecular layer	HPF	Hippocampal formation	11	26
DG-po	Dentate gyrus polymorph layer	HPF	Hippocampal formation	11	26
DG-sg	Dentate gyrus granule cell layer	HPF	Hippocampal formation	11	26
FC	Fasciola cinerea	HPF	Hippocampal formation	9	-1
IG	Induseum griseum	HPF	Hippocampal formation	17	1
ENTl1	Entorhinal area lateral part layer 1	HPF	Hippocampal formation	-1	-1

Allen acronym	Allen name	Cosmos acronym	Cosmos name	Inter-trial	Audio-visual cue
ENTl2	Entorhinal area lateral part layer 2	HPF	Hippocampal formation	29	-1
ENTl3	Entorhinal area lateral part layer 3	HPF	Hippocampal formation	29	11
ENTl5	Entorhinal area lateral part layer 5	HPF	Hippocampal formation	9	11
ENTl6a	Entorhinal area lateral part layer 6a	HPF	Hippocampal formation	-1	-1
ENTm1	Entorhinal area medial part dorsal zone layer 1	HPF	Hippocampal formation	-1	-1
ENTm2	Entorhinal area medial part dorsal zone layer 2	HPF	Hippocampal formation	-1	-1
ENTm3	Entorhinal area medial part dorsal zone layer 3	HPF	Hippocampal formation	9	-1
ENTm5	Entorhinal area medial part dorsal zone layer 5	HPF	Hippocampal formation	9	12
ENTm6	Entorhinal area medial part dorsal zone layer 6	HPF	Hippocampal formation	9	12
HATA	Hippocampo-amygdalar transition area	HPF	Hippocampal formation	-1	34
APr	Area prostriata	HPF	Hippocampal formation	3	7
CLA	Claustrum	CTXsp	Cortical subplate	2	2
EPd	Endopiriform nucleus dorsal part	CTXsp	Cortical subplate	2	-1
EPv	Endopiriform nucleus ventral part	CTXsp	Cortical subplate	10	13
LA	Lateral amygdalar nucleus	CTXsp	Cortical subplate	28	14
BLAa	Basolateral amygdalar nucleus anterior part	CTXsp	Cortical subplate	28	-1
BLAp	Basolateral amygdalar nucleus posterior part	CTXsp	Cortical subplate	-1	13
BLAv	Basolateral amygdalar nucleus ventral part	CTXsp	Cortical subplate	-1	-1
BMAa	Basomedial amygdalar nucleus anterior part	CTXsp	Cortical subplate	28	14
BMAp	Basomedial amygdalar nucleus posterior part	CTXsp	Cortical subplate	-1	14
PA	Posterior amygdalar nucleus	CTXsp	Cortical subplate	9	-1
CP	Caudoputamen	CNU	Cerebral nuclei	2	1
ACB	Nucleus accumbens	CNU	Cerebral nuclei	2	-1
FS	Fundus of striatum	CNU	Cerebral nuclei	-1	14
LSc	Lateral septal nucleus caudal (caudodorsal) part	CNU	Cerebral nuclei	-1	3
LSr	Lateral septal nucleus rostral (rostroventral) part	CNU	Cerebral nuclei	18	3

Allen acronym	Allen name	Cosmos acronym	Cosmos name	Inter-trial	Audio-visual cue
LSv	Lateral septal nucleus ventral part	CNU	Cerebral nuclei	18	3
SF	Septofimbrial nucleus	CNU	Cerebral nuclei	12	3
SH	Septohippocampal nucleus	CNU	Cerebral nuclei	18	3
AAA	Anterior amygdalar area	CNU	Cerebral nuclei	-1	-1
CEAc	Central amygdalar nucleus capsular part	CNU	Cerebral nuclei	-1	14
CEAl	Central amygdalar nucleus lateral part	CNU	Cerebral nuclei	-1	14
CEAm	Central amygdalar nucleus medial part	CNU	Cerebral nuclei	-1	14
IA	Intercalated amygdalar nucleus	CNU	Cerebral nuclei	-1	14
GPe	Globus pallidus external segment	CNU	Cerebral nuclei	-1	-1
GPi	Globus pallidus internal segment	CNU	Cerebral nuclei	28	14
SI	Substantia innominata	CNU	Cerebral nuclei	18	-1
MA	Magnocellular nucleus	CNU	Cerebral nuclei	-1	-1
MS	Medial septal nucleus	CNU	Cerebral nuclei	18	-1
NDB	Diagonal band nucleus	CNU	Cerebral nuclei	18	-1
TRS	Triangular nucleus of septum	CNU	Cerebral nuclei	12	3
VAL	Ventral anterior-lateral complex of the thalamus	TH	Thalamus	19	17
VM	Ventral medial nucleus of the thalamus	TH	Thalamus	19	18
VPL	Ventral posterolateral nucleus of the thalamus	TH	Thalamus	-1	10
VPLpc	Ventral posterolateral nucleus of the thalamus parvicellular part	TH	Thalamus	19	10
VPM	Ventral posteromedial nucleus of the thalamus	TH	Thalamus	19	10
VPMpc	Ventral posteromedial nucleus of the thalamus parvicellular part	TH	Thalamus	-1	18
PoT	Posterior triangular thalamic nucleus	TH	Thalamus	19	10
SPFm	Subparafascicular nucleus magnocellular part	TH	Thalamus	13	15
SPFp	Subparafascicular nucleus parvicellular part	TH	Thalamus	-1	10
SPA	Subparafascicular area	TH	Thalamus	13	16
PP	Peripeduncular nucleus	TH	Thalamus	-1	-1
MGd	Medial geniculate complex dorsal part	TH	Thalamus	9	-1

Allen acronym	Allen name	Cosmos acronym	Cosmos name	Inter-trial	Audio-visual cue
MGv	Medial geniculate complex ventral part	TH	Thalamus	-1	29
MGm	Medial geniculate complex medial part	TH	Thalamus	12	10
LGd-sh	Dorsal part of the lateral geniculate complex shell	TH	Thalamus	-1	-1
LGd-co	Dorsal part of the lateral geniculate complex core	TH	Thalamus	-1	29
LGd-ip	Dorsal part of the lateral geniculate complex ipsilateral zone	TH	Thalamus	-1	29
LP	Lateral posterior nucleus of the thalamus	TH	Thalamus	19	10
PO	Posterior complex of the thalamus	TH	Thalamus	19	10
POL	Posterior limiting nucleus of the thalamus	TH	Thalamus	12	-1
SGN	Suprageniculate nucleus	TH	Thalamus	19	10
Eth	Ethmoid nucleus of the thalamus	TH	Thalamus	19	-1
AV	Anteroventral nucleus of thalamus	TH	Thalamus	12	17
AMd	Anteromedial nucleus dorsal part	TH	Thalamus	12	-1
AMv	Anteromedial nucleus ventral part	TH	Thalamus	-1	-1
AD	Anterodorsal nucleus	TH	Thalamus	-1	-1
IAM	Interanteromedial nucleus of the thalamus	TH	Thalamus	12	15
IAD	Interanterodorsal nucleus of the thalamus	TH	Thalamus	12	-1
LD	Lateral dorsal nucleus of thalamus	TH	Thalamus	19	10
IMD	Intermediodorsal nucleus of the thalamus	TH	Thalamus	13	15
SMT	Submedial nucleus of the thalamus	TH	Thalamus	12	17
PR	Perireunensis nucleus	TH	Thalamus	12	16
PVT	Paraventricular nucleus of the thalamus	TH	Thalamus	12	15
PT	Parataenial nucleus	TH	Thalamus	12	15
RE	Nucleus of reuniens	TH	Thalamus	12	15
Xi	Xiphoid thalamic nucleus	TH	Thalamus	12	15
RH	Rhomboid nucleus	TH	Thalamus	12	15
CM	Central medial nucleus of the thalamus	TH	Thalamus	-1	-1
PCN	Paracentral nucleus	TH	Thalamus	12	17
CL	Central lateral nucleus of the thalamus	TH	Thalamus	19	-1
PF	Parafascicular nucleus	TH	Thalamus	22	-1
PIL	Posterior intralaminar thalamic nucleus	TH	Thalamus	14	10
RT	Reticular nucleus of the thalamus	TH	Thalamus	-1	-1
IGL	Intergeniculate leaflet of the lateral geniculate complex	TH	Thalamus	-1	29
IntG	Intermediate geniculate nucleus	TH	Thalamus	-1	-1
SubG	Subgeniculate nucleus	TH	Thalamus	-1	-1
MH	Medial habenula	TH	Thalamus	13	18
LH	Lateral habenula	TH	Thalamus	-1	-1
ADP	Anterodorsal preoptic nucleus	HY	Hypothalamus	18	-1
AVP	Anteroventral preoptic nucleus	HY	Hypothalamus	18	33

Allen acronym	Allen name	Cosmos acronym	Cosmos name	Inter-trial	Audio-visual cue
MPO	Medial preoptic area	HY	Hypothalamus	18	33
PS	Parastrial nucleus	HY	Hypothalamus	-1	33
SFO	Subfornical organ	HY	Hypothalamus	-1	3
VLPO	Ventrolateral preoptic nucleus	HY	Hypothalamus	-1	33
LM	Lateral mammillary nucleus	HY	Hypothalamus	-1	-1
Mml	Medial mammillary nucleus lateral part	HY	Hypothalamus	-1	-1
PH	Posterior hypothalamic nucleus	HY	Hypothalamus	13	15
LHA	Lateral hypothalamic area	HY	Hypothalamus	12	-1
LPO	Lateral preoptic area	HY	Hypothalamus	-1	33
PeF	Perifornical nucleus	HY	Hypothalamus	12	18
STN	Subthalamic nucleus	HY	Hypothalamus	25	10
TU	Tuberal nucleus	HY	Hypothalamus	12	10
FF	Fields of Forel	HY	Hypothalamus	-1	10
SCop	Superior colliculus optic layer	MB	Midbrain	3	7
SCsg	Superior colliculus superficial gray layer	MB	Midbrain	3	7
SCzo	Superior colliculus zonal layer	MB	Midbrain	3	7
ICc	Inferior colliculus central nucleus	MB	Midbrain	1	-1
ICd	Inferior colliculus dorsal nucleus	MB	Midbrain	-1	-1
ICe	Inferior colliculus external nucleus	MB	Midbrain	-1	27
NB	Nucleus of the brachium of the inferior colliculus	MB	Midbrain	14	10
SAG	Nucleus sagulum	MB	Midbrain	-1	-1
PBG	Parabigeminal nucleus	MB	Midbrain	-1	-1
SNr	Substantia nigra reticular part	MB	Midbrain	14	10
VTA	Ventral tegmental area	MB	Midbrain	14	-1
RR	Midbrain reticular nucleus retrorubral area	MB	Midbrain	-1	-1
SCdg	Superior colliculus motor related deep gray layer	MB	Midbrain	12	10
SCdw	Superior colliculus motor related deep white layer	MB	Midbrain	12	10
SCiw	Superior colliculus motor related intermediate white layer	MB	Midbrain	14	10
PRC	Precommissural nucleus	MB	Midbrain	13	16
INC	Interstitial nucleus of Cajal	MB	Midbrain	-1	10
ND	Nucleus of Darkschewitsch	MB	Midbrain	14	10
Su3	Supraoculomotor periaqueductal gray	MB	Midbrain	-1	10
APN	Anterior pretectal nucleus	MB	Midbrain	14	10
MPT	Medial pretectal area	MB	Midbrain	-1	-1
NOT	Nucleus of the optic tract	MB	Midbrain	14	10
NPC	Nucleus of the posterior commissure	MB	Midbrain	14	10
OP	Olivary pretectal nucleus	MB	Midbrain	14	10
PPT	Posterior pretectal nucleus	MB	Midbrain	14	10
RPF	Retroparafascicular nucleus	MB	Midbrain	14	10
CUN	Cuneiform nucleus	MB	Midbrain	1	27
RN	Red nucleus	MB	Midbrain	15	10
III	Oculomotor nucleus	MB	Midbrain	14	10
MA3	Medial accesory oculomotor nucleus	MB	Midbrain	-1	-1
EW	Edinger-Westphal nucleus	MB	Midbrain	-1	-1
Pa4	Paratrochlear nucleus	MB	Midbrain	14	10

Allen acronym	Allen name	Cosmos acronym	Cosmos name	Inter-trial	Audio-visual cue
VTN	Ventral tegmental nucleus	MB	Midbrain	15	10
AT	Anterior tegmental nucleus	MB	Midbrain	16	32
DT	Dorsal terminal nucleus of the accessory optic tract	MB	Midbrain	8	-1
MT	Medial terminal nucleus of the accessory optic tract	MB	Midbrain	14	-1
SNc	Substantia nigra compact part	MB	Midbrain	14	10
PPN	Pedunculopontine nucleus	MB	Midbrain	-1	-1
IF	Interfascicular nucleus raphe	MB	Midbrain	15	10
IPA	Interpeduncular nucleus apical	MB	Midbrain	14	10
IPL	Interpeduncular nucleus lateral	MB	Midbrain	12	-1
IPDM	Interpeduncular nucleus dorsomedial	MB	Midbrain	15	10
IPDL	Interpeduncular nucleus dorsolateral	MB	Midbrain	14	10
RL	Rostral linear nucleus raphe	MB	Midbrain	14	10
CLI	Central linear nucleus raphe	MB	Midbrain	14	10
DR	Dorsal nucleus raphe	MB	Midbrain	-1	10
PSV	Principal sensory nucleus of the trigeminal	HB	Hindbrain	-1	28
KF	Koelliker-Fuse subnucleus	HB	Hindbrain	0	9
POR	Superior olivary complex periolivary region	HB	Hindbrain	-1	-1
SOCm	Superior olivary complex medial part	HB	Hindbrain	-1	32
SOCl	Superior olivary complex lateral part	HB	Hindbrain	1	-1
DTN	Dorsal tegmental nucleus	HB	Hindbrain	-1	-1
PDTg	Posterodorsal tegmental nucleus	HB	Hindbrain	-1	-1
PCG	Pontine central gray	HB	Hindbrain	-1	-1
PG	Pontine gray	HB	Hindbrain	-1	-1
PRNc	Pontine reticular nucleus caudal part	HB	Hindbrain	1	-1
SUT	Supratrigeminal nucleus	HB	Hindbrain	1	28
TRN	Tegmental reticular nucleus	HB	Hindbrain	16	-1
V	Motor nucleus of trigeminal	HB	Hindbrain	-1	28
P5	Peritrigeminal zone	HB	Hindbrain	-1	-1
PC5	Parvicellular motor 5 nucleus	HB	Hindbrain	1	28
I5	Intertrigeminal nucleus	HB	Hindbrain	0	-1
LC	Locus ceruleus	HB	Hindbrain	-1	-1
LDT	Laterodorsal tegmental nucleus	HB	Hindbrain	-1	-1
NI	Nucleus incertus	HB	Hindbrain	-1	-1
PRNr	Pontine reticular nucleus	HB	Hindbrain	-1	32
DCO	Dorsal cochlear nucleus	HB	Hindbrain	0	9
VCO	Ventral cochlear nucleus	HB	Hindbrain	0	-1
CU	Cuneate nucleus	HB	Hindbrain	0	-1
ECU	External cuneate nucleus	HB	Hindbrain	0	9
SPVC	Spinal nucleus of the trigeminal caudal part	HB	Hindbrain	0	9
SPVI	Spinal nucleus of the trigeminal interpolar part	HB	Hindbrain	0	9
Pa5	Paratrigeminal nucleus	HB	Hindbrain	0	9
VII	Facial motor nucleus	HB	Hindbrain	-1	-1

Allen acronym	Allen name	Cosmos acronym	Cosmos name	Inter-trial	Audio-visual cue
AMBv	Nucleus ambiguus ventral division	HB	Hindbrain	0	9
DMX	Dorsal motor nucleus of the vagus nerve	HB	Hindbrain	-1	9
GRN	Gigantocellular reticular nucleus	HB	Hindbrain	0	9
ICB	Infracerebellar nucleus	HB	Hindbrain	0	9
IO	Inferior olivary complex	HB	Hindbrain	0	9
IRN	Intermediate reticular nucleus	HB	Hindbrain	0	9
LIN	Linear nucleus of the medulla	HB	Hindbrain	0	9
LRNm	Lateral reticular nucleus magnocellular part	HB	Hindbrain	0	9
MARN	Magnocellular reticular nucleus	HB	Hindbrain	0	9
MDRNd	Medullary reticular nucleus dorsal part	HB	Hindbrain	0	9
MDRNv	Medullary reticular nucleus ventral part	HB	Hindbrain	0	9
PARN	Parvicellular reticular nucleus	HB	Hindbrain	0	9
PAS	Parasolitary nucleus	HB	Hindbrain	0	-1
PGRNd	Paragigantocellular reticular nucleus dorsal part	HB	Hindbrain	0	9
PGRNl	Paragigantocellular reticular nucleus lateral part	HB	Hindbrain	0	9
PRP	Nucleus prepositus	HB	Hindbrain	0	9
LAV	Lateral vestibular nucleus	HB	Hindbrain	0	9
MV	Medial vestibular nucleus	HB	Hindbrain	0	9
SPIV	Spinal vestibular nucleus	HB	Hindbrain	0	9
SUV	Superior vestibular nucleus	HB	Hindbrain	-1	9
x	Nucleus x	HB	Hindbrain	0	9
XII	Hypoglossal nucleus	HB	Hindbrain	30	34
y	Nucleus y	HB	Hindbrain	0	9
RO	Nucleus raphe obscurus	HB	Hindbrain	30	34
FN	Fastigial nucleus	CB	Cerebellum	0	9
IP	Interposed nucleus	CB	Cerebellum	0	9
DN	Dentate nucleus	CB	Cerebellum	0	9
VeCB	Vestibulocerebellar nucleus	CB	Cerebellum	0	9
MOB	Main olfactory bulb	OLF	Olfactory areas	-1	-1
AON	Anterior olfactory nucleus	OLF	Olfactory areas	10	26
TTd	Taenia tecta dorsal part	OLF	Olfactory areas	-1	-1
TTv	Taenia tecta ventral part	OLF	Olfactory areas	-1	-1
DP	Dorsal peduncular area	OLF	Olfactory areas	7	-1
PIR	Piriform area	OLF	Olfactory areas	-1	11
COAa	Cortical amygdalar area anterior part	OLF	Olfactory areas	28	14
COAp	Cortical amygdalar area posterior part	OLF	Olfactory areas	-1	-1
PAA	Piriform-amygdalar area	OLF	Olfactory areas	28	14

Allen acronym	Allen name	Cosmos acronym	Cosmos name	Inter-trial	Audio-visual cue
TR	Postpiriform transition area	OLF	Olfactory areas	9	13
CA1	Field CA1	HPF	Hippocampal formation	9	-1
CA2	Field CA2	HPF	Hippocampal formation	9	-1
CA3	Field CA3	HPF	Hippocampal formation	9	-1
PAR	Parasubiculum	HPF	Hippocampal formation	-1	-1
POST	Postsubiculum	HPF	Hippocampal formation	4	7
PRE	Presubiculum	HPF	Hippocampal formation	-1	-1
SUB	Subiculum	HPF	Hippocampal formation	-1	-1
ProS	Prosubiculum	HPF	Hippocampal formation	9	26
OT	Olfactory tubercle	CNU	Cerebral nuclei	-1	-1
MEA	Medial amygdalar nucleus	CNU	Cerebral nuclei	-1	14
BST	Bed nuclei of the stria terminalis	CNU	Cerebral nuclei	18	3
MD	Mediodorsal nucleus of thalamus	TH	Thalamus	13	-1
LGv	Ventral part of the lateral geniculate complex	TH	Thalamus	10	-1
PVH	Paraventricular hypothalamic nucleus	HY	Hypothalamus	12	15
DMH	Dorsomedial nucleus of the hypothalamus	HY	Hypothalamus	13	15
AHN	Anterior hypothalamic nucleus	HY	Hypothalamus	12	15
SUM	Supramammillary nucleus	HY	Hypothalamus	13	-1
MPN	Medial preoptic nucleus	HY	Hypothalamus	12	15
PVHd	Paraventricular hypothalamic nucleus descending division	HY	Hypothalamus	12	16
VMH	Ventromedial hypothalamic nucleus	HY	Hypothalamus	13	15
MRN	Midbrain reticular nucleus	MB	Midbrain	14	10
NLL	Nucleus of the lateral lemniscus	HB	Hindbrain	30	27
CS	Superior central nucleus raphe	HB	Hindbrain	16	10
NTS	Nucleus of the solitary tract	HB	Hindbrain	0	9
SPVO	Spinal nucleus of the trigeminal oral part	HB	Hindbrain	0	9
LING	Lingula (I)	CB	Cerebellum	0	9
CENT2	Lobule II	CB	Cerebellum	0	9
CENT3	Lobule III	CB	Cerebellum	0	9
CUL4 5	Lobules IV-V	CB	Cerebellum	0	9
DEC	Declive (VI)	CB	Cerebellum	0	9
FOTU	Folium-tuber vermis (VII)	CB	Cerebellum	0	9
PYR	Pyramus (VIII)	CB	Cerebellum	0	9
UVU	Uvula (IX)	CB	Cerebellum	0	9
NOD	Nodulus (X)	CB	Cerebellum	0	9
SIM	Simple lobule	CB	Cerebellum	0	9

Allen acronym	**Allen name**	**Cosmos acronym**	**Cosmos name**	**Inter-trial**	**Audio-visual cue**
ANcr1	Crus 1	CB	Cerebellum	0	12
ANcr2	Crus 2	CB	Cerebellum	0	9
PRM	Paramedian lobule	CB	Cerebellum	0	9
COPY	Copula pyramidis	CB	Cerebellum	0	9
PFL	Paraflocculus	CB	Cerebellum	0	9
FL	Flocculus	CB	Cerebellum	0	9

Supplementary Table 3: Table for community hub.

Allen acronym	**Allen name**	**inter-trial commu-nity**	**inter-trial hub**	**Audio-visual cue com-mu-nity**	**Audio-visual cue hub**
FRP1	Frontal pole layer 1	10	AON	26	ProS
FRP2/3	Frontal pole layer 2/3	10	AON	26	ProS
FRP5	Frontal pole layer 5	-1	N/A	1	CP
FRP6a	Frontal pole layer 6a	2	CP	1	CP
MOp1	Primary motor area Layer 1	-1	N/A	-1	N/A
MOp2/3	Primary motor area Layer 2/3	-1	N/A	-1	N/A
MOp5	Primary motor area Layer 5	2	CP	2	MOp6a
MOp6a	Primary motor area Layer 6a	2	CP	2	MOp6a
MOp6b	Primary motor area Layer 6b	2	CP	2	MOp6a
MOs1	Secondary motor area layer 1	-1	N/A	-1	N/A
MOs2/3	Secondary motor area layer 2/3	-1	N/A	-1	N/A
MOs5	Secondary motor area layer 5	-1	N/A	1	CP
MOs6a	Secondary motor area layer 6a	2	CP	1	CP
MOs6b	Secondary motor area layer 6b	2	CP	1	CP
SSp-n1	Primary somatosensory area nose layer 1	-1	N/A	-1	N/A
SSp-n2/3	Primary somatosensory area nose layer 2/3	-1	N/A	1	CP
SSp-n4	Primary somatosensory area nose layer 4	-1	N/A	2	MOp6a
SSp-n5	Primary somatosensory area nose layer 5	-1	N/A	-1	N/A
SSp-n6a	Primary somatosensory area nose layer 6a	-1	N/A	2	MOp6a
SSp-n6b	Primary somatosensory area nose layer 6b	-1	N/A	2	MOp6a
SSp-bfd1	Primary somatosensory area barrel field layer 1	6	VISl5	-1	N/A
SSp-bfd2/3	Primary somatosensory area barrel field layer 2/3	6	VISl5	0	SSp-bfd2/3
SSp-bfd4	Primary somatosensory area barrel field layer 4	5	SSp-bfd5	24	SSs5
SSp-bfd5	Primary somatosensory area barrel field layer 5	5	SSp-bfd5	-1	N/A
SSp-bfd6a	Primary somatosensory area barrel field layer 6a	24	SSp-bfd6a	-1	N/A
SSp-bfd6b	Primary somatosensory area barrel field layer 6b	24	SSp-bfd6a	-1	N/A
SSp-ll1	Primary somatosensory area lower limb layer 1	4	POST	20	SSp-ul5
SSp-ll2/3	Primary somatosensory area lower limb layer 2/3	4	POST	20	SSp-ul5
SSp-ll4	Primary somatosensory area lower limb layer 4	-1	N/A	20	SSp-ul5
SSp-ll5	Primary somatosensory area lower limb layer 5	-1	N/A	20	SSp-ul5

Allen acronym	Allen name	inter-trial commu-nity	inter-trial hub	Audio-visual cue com-mu-nity	Audio-visual cue hub
SSp-ll6a	Primary somatosensory area lower limb layer 6a	23	SSp-tr5	20	SSp-ul5
SSp-ll6b	Primary somatosensory area lower limb layer 6b	23	SSp-tr5	20	SSp-ul5
SSp-m1	Primary somatosensory area mouth layer 1	-1	N/A	-1	N/A
SSp-m2/3	Primary somatosensory area mouth layer 2/3	2	CP	22	SSp-m5
SSp-m4	Primary somatosensory area mouth layer 4	2	CP	22	SSp-m5
SSp-m5	Primary somatosensory area mouth layer 5	2	CP	22	SSp-m5
SSp-m6a	Primary somatosensory area mouth layer 6a	2	CP	2	MOp6a
SSp-m6b	Primary somatosensory area mouth layer 6b	2	CP	2	MOp6a
SSp-ul1	Primary somatosensory area upper limb layer 1	23	SSp-tr5	20	SSp-ul5
SSp-ul2/3	Primary somatosensory area upper limb layer 2/3	-1	N/A	20	SSp-ul5
SSp-ul4	Primary somatosensory area upper limb layer 4	-1	N/A	20	SSp-ul5
SSp-ul5	Primary somatosensory area upper limb layer 5	17	SSp-ul5	20	SSp-ul5
SSp-ul6a	Primary somatosensory area upper limb layer 6a	-1	N/A	20	SSp-ul5
SSp-ul6b	Primary somatosensory area upper limb layer 6b	-1	N/A	20	SSp-ul5
SSp-tr1	Primary somatosensory area trunk layer 1	4	POST	-1	N/A
SSp-tr2/3	Primary somatosensory area trunk layer 2/3	23	SSp-tr5	19	SSp-tr5
SSp-tr4	Primary somatosensory area trunk layer 4	23	SSp-tr5	19	SSp-tr5
SSp-tr5	Primary somatosensory area trunk layer 5	23	SSp-tr5	19	SSp-tr5
SSp-tr6a	Primary somatosensory area trunk layer 6a	24	SSp-bfd6a	19	SSp-tr5
SSp-tr6b	Primary somatosensory area trunk layer 6b	24	SSp-bfd6a	19	SSp-tr5
SSp-un1	Primary somatosensory area unassigned layer 1	14	APN	-1	N/A
SSp-un2/3	Primary somatosensory area unassigned layer 2/3	24	SSp-bfd6a	-1	N/A
SSp-un4	Primary somatosensory area unassigned layer 4	24	SSp-bfd6a	-1	N/A
SSp-un5	Primary somatosensory area unassigned layer 5	24	SSp-bfd6a	-1	N/A
SSp-un6a	Primary somatosensory area unassigned layer 6a	-1	N/A	-1	N/A

Allen acronym	Allen name	inter-trial commu-nity	inter-trial hub	Audio-visual cue com-mu-nity	Audio-visual cue hub
SSp-un6b	Primary somatosensory area unassigned layer 6b	-1	N/A	-1	N/A
SSs2/3	Supplemental somatosensory area layer 2/3	6	VISl5	6	VISp2/3
SSs4	Supplemental somatosensory area layer 4	6	VISl5	-1	N/A
SSs5	Supplemental somatosensory area layer 5	21	SSs5	24	SSs5
SSs6a	Supplemental somatosensory area layer 6a	-1	N/A	23	SSs6a
SSs6b	Supplemental somatosensory area layer 6b	-1	N/A	23	SSs6a
GU5	Gustatory areas layer 5	2	CP	22	SSp-m5
GU6a	Gustatory areas layer 6a	2	CP	22	SSp-m5
VISC5	Visceral area layer 5	20	VISC5	25	VISC5
VISC6a	Visceral area layer 6a	-1	N/A	23	SSs6a
VISC6b	Visceral area layer 6b	-1	N/A	1	CP
AUDd2/3	Dorsal auditory area layer 2/3	-1	N/A	-1	N/A
AUDd4	Dorsal auditory area layer 4	-1	N/A	-1	N/A
AUDd5	Dorsal auditory area layer 5	21	SSs5	-1	N/A
AUDd6a	Dorsal auditory area layer 6a	21	SSs5	24	SSs5
AUDd6b	Dorsal auditory area layer 6b	-1	N/A	-1	N/A
AUDp4	Primary auditory area layer 4	-1	N/A	-1	N/A
AUDp5	Primary auditory area layer 5	-1	N/A	-1	N/A
AUDp6a	Primary auditory area layer 6a	21	SSs5	-1	N/A
AUDpo2/3	Posterior auditory area layer 2/3	-1	N/A	-1	N/A
AUDpo4	Posterior auditory area layer 4	-1	N/A	-1	N/A
AUDpo5	Posterior auditory area layer 5	21	SSs5	21	VISrl5
AUDpo6a	Posterior auditory area layer 6a	21	SSs5	21	VISrl5
AUDpo6b	Posterior auditory area layer 6b	21	SSs5	-1	N/A
AUDv5	Ventral auditory area layer 5	-1	N/A	-1	N/A
AUDv6a	Ventral auditory area layer 6a	21	SSs5	21	VISrl5
AUDv6b	Ventral auditory area layer 6b	-1	N/A	-1	N/A
VISal2/3	Anterolateral visual area layer 2/3	21	SSs5	21	VISrl5
VISal4	Anterolateral visual area layer 4	21	SSs5	21	VISrl5
VISal5	Anterolateral visual area layer 5	-1	N/A	-1	N/A
VISal6a	Anterolateral visual area layer 6a	22	PF	21	VISrl5
VISal6b	Anterolateral visual area layer 6b	22	PF	21	VISrl5
VISam1	Anteromedial visual area layer 1	4	POST	31	VISam6a
VISam2/3	Anteromedial visual area layer 2/3	27	VISa4	31	VISam6a
VISam4	Anteromedial visual area layer 4	27	VISa4	31	VISam6a
VISam5	Anteromedial visual area layer 5	27	VISa4	31	VISam6a
VISam6a	Anteromedial visual area layer 6a	27	VISa4	31	VISam6a
VISam6b	Anteromedial visual area layer 6b	27	VISa4	31	VISam6a
VISl1	Lateral visual area layer 1	6	VISl5	8	VISl5
VISl2/3	Lateral visual area layer 2/3	6	VISl5	8	VISl5

Allen acronym	Allen name	inter-trial commu-nity	inter-trial hub	Audio-visual cue com-mu-nity	Audio-visual cue hub
VISl4	Lateral visual area layer 4	6	VISl5	8	VISl5
VISl5	Lateral visual area layer 5	6	VISl5	8	VISl5
VISl6a	Lateral visual area layer 6a	-1	N/A	8	VISl5
VISl6b	Lateral visual area layer 6b	-1	N/A	-1	N/A
VISp1	Primary visual area layer 1	3	VISp5	7	POST
VISp2/3	Primary visual area layer 2/3	3	VISp5	6	VISp2/3
VISp4	Primary visual area layer 4	3	VISp5	7	POST
VISp5	Primary visual area layer 5	3	VISp5	7	POST
VISp6a	Primary visual area layer 6a	3	VISp5	-1	N/A
VISp6b	Primary visual area layer 6b	-1	N/A	-1	N/A
VISpl1	Posterolateral visual area layer 1	5	SSp-bfd5	-1	N/A
VISpl2/3	Posterolateral visual area layer 2/3	-1	N/A	-1	N/A
VISpl4	Posterolateral visual area layer 4	-1	N/A	-1	N/A
VISpl5	Posterolateral visual area layer 5	3	VISp5	7	POST
VISpl6a	Posterolateral visual area layer 6a	3	VISp5	6	VISp2/3
VISpm1	posteromedial visual area layer 1	4	POST	7	POST
VISpm2/3	posteromedial visual area layer 2/3	4	POST	7	POST
VISpm4	posteromedial visual area layer 4	4	POST	7	POST
VISpm5	posteromedial visual area layer 5	4	POST	5	VISpm5
VISpm6a	posteromedial visual area layer 6a	27	VISa4	5	VISpm5
VISpm6b	posteromedial visual area layer 6b	-1	N/A	5	VISpm5
VISli2/3	Laterointermediate area layer 2/3	3	VISp5	8	VISl5
VISli4	Laterointermediate area layer 4	-1	N/A	-1	N/A
VISli5	Laterointermediate area layer 5	6	VISl5	-1	N/A
VISli6a	Laterointermediate area layer 6a	8	VISli6a	-1	N/A
VISli6b	Laterointermediate area layer 6b	9	CA1	8	VISl5
VISpor1	Postrhinal area layer 1	-1	N/A	12	ANcr1
VISpor2/3	Postrhinal area layer 2/3	-1	N/A	12	ANcr1
VISpor5	Postrhinal area layer 5	17	SSp-ul5	-1	N/A
VISpor6a	Postrhinal area layer 6a	17	SSp-ul5	-1	N/A
VISpor6b	Postrhinal area layer 6b	12	SCdg	-1	N/A
ACAd2/3	Anterior cingulate area dorsal part layer 2/3	31	PL1	-1	N/A
ACAd5	Anterior cingulate area dorsal part layer 5	2	CP	1	CP
ACAd6a	Anterior cingulate area dorsal part layer 6a	2	CP	1	CP
ACAd6b	Anterior cingulate area dorsal part layer 6b	2	CP	1	CP
ACAv1	Anterior cingulate area ventral part layer 1	17	SSp-ul5	1	CP
ACAv2/3	Anterior cingulate area ventral part layer 2/3	2	CP	1	CP

Allen acronym	Allen name	inter-trial commu-nity	inter-trial hub	Audio-visual cue com-mu-nity	Audio-visual cue hub
ACAv5	Anterior cingulate area ventral part layer 5	2	CP	1	CP
ACAv6a	Anterior cingulate area ventral part 6a	2	CP	1	CP
ACAv6b	Anterior cingulate area ventral part 6b	2	CP	1	CP
PL1	Prelimbic area layer 1	31	PL1	30	PL1
PL2/3	Prelimbic area layer 2/3	31	PL1	30	PL1
PL5	Prelimbic area layer 5	2	CP	4	ORBvl6a
PL6a	Prelimbic area layer 6a	2	CP	1	CP
PL6b	Prelimbic area layer 6b	2	CP	1	CP
ILA1	Infralimbic area layer 1	2	CP	4	ORBvl6a
ILA2/3	Infralimbic area layer 2/3	2	CP	4	ORBvl6a
ILA5	Infralimbic area layer 5	2	CP	4	ORBvl6a
ILA6a	Infralimbic area layer 6a	2	CP	1	CP
ORBl1	Orbital area lateral part layer 1	10	AON	26	ProS
ORBl2/3	Orbital area lateral part layer 2/3	10	AON	26	ProS
ORBl5	Orbital area lateral part layer 5	7	DP	2	MOp6a
ORBl6a	Orbital area lateral part layer 6a	2	CP	2	MOp6a
ORBm1	Orbital area medial part layer 1	31	PL1	30	PL1
ORBm2/3	Orbital area medial part layer 2/3	7	DP	-1	N/A
ORBm5	Orbital area medial part layer 5	2	CP	4	ORBvl6a
ORBm6a	Orbital area medial part layer 6a	2	CP	4	ORBvl6a
ORBvl1	Orbital area ventrolateral part layer 1	10	AON	26	ProS
ORBvl2/3	Orbital area ventrolateral part layer 2/3	10	AON	26	ProS
ORBvl5	Orbital area ventrolateral part layer 5	-1	N/A	-1	N/A
ORBvl6a	Orbital area ventrolateral part layer 6a	2	CP	4	ORBvl6a
AId5	Agranular insular area dorsal part layer 5	2	CP	-1	N/A
AId6a	Agranular insular area dorsal part layer 6a	2	CP	2	MOp6a
AId6b	Agranular insular area dorsal part layer 6b	2	CP	2	MOp6a
AIp1	Agranular insular area posterior part layer 1	-1	N/A	23	SSs6a
AIp2/3	Agranular insular area posterior part layer 2/3	20	VISC5	25	VISC5
AIp5	Agranular insular area posterior part layer 5	20	VISC5	25	VISC5
AIp6a	Agranular insular area posterior part layer 6a	-1	N/A	-1	N/A
AIp6b	Agranular insular area posterior part layer 6b	2	CP	1	CP

Allen acronym	Allen name	inter-trial commu-nity	inter-trial hub	Audio-visual cue com-mu-nity	Audio-visual cue hub
AIv2/3	Agranular insular area ventral part layer 2/3	2	CP	-1	N/A
AIv5	Agranular insular area ventral part layer 5	2	CP	2	MOp6a
AIv6a	Agranular insular area ventral part layer 6a	2	CP	2	MOp6a
AIv6b	Agranular insular area ventral part layer 6b	2	CP	2	MOp6a
RSPagl1	Retrosplenial area lateral agranular part layer 1	4	POST	-1	N/A
RSPagl2/3	Retrosplenial area lateral agranular part layer 2/3	4	POST	7	POST
RSPagl5	Retrosplenial area lateral agranular part layer 5	3	VISp5	7	POST
RSPagl6a	Retrosplenial area lateral agranular part layer 6a	3	VISp5	7	POST
RSPagl6b	Retrosplenial area lateral agranular part layer 6b	-1	N/A	7	POST
RSPd1	Retrosplenial area dorsal part layer 1	-1	N/A	7	POST
RSPd2/3	Retrosplenial area dorsal part layer 2/3	4	POST	7	POST
RSPd5	Retrosplenial area dorsal part layer 5	3	VISp5	7	POST
RSPd6a	Retrosplenial area dorsal part layer 6a	3	VISp5	7	POST
RSPd6b	Retrosplenial area dorsal part layer 6b	4	POST	5	VISpm5
RSPv1	Retrosplenial area ventral part layer 1	3	VISp5	-1	N/A
RSPv2/3	Retrosplenial area ventral part layer 2/3	-1	N/A	7	POST
RSPv5	Retrosplenial area ventral part layer 5	-1	N/A	-1	N/A
RSPv6a	Retrosplenial area ventral part layer 6a	-1	N/A	6	VISp2/3
RSPv6b	Retrosplenial area ventral part layer 6b	-1	N/A	5	VISpm5
VISa1	Anterior area layer 1	6	VISl5	-1	N/A
VISa2/3	Anterior area layer 2/3	4	POST	7	POST
VISa4	Anterior area layer 4	27	VISa4	7	POST
VISa5	Anterior area layer 5	25	VISa5	7	POST
VISa6a	Anterior area layer 6a	25	VISa5	-1	N/A
VISa6b	Anterior area layer 6b	25	VISa5	7	POST
VISrl1	Rostrolateral area layer 1	21	SSs5	21	VISrl5
VISrl2/3	Rostrolateral area layer 2/3	26	VISrl2/3	21	VISrl5
VISrl4	Rostrolateral area layer 4	26	VISrl2/3	-1	N/A
VISrl5	Rostrolateral area layer 5	26	VISrl2/3	21	VISrl5
VISrl6a	Rostrolateral area layer 6a	25	VISa5	21	VISrl5
VISrl6b	Rostrolateral area layer 6b	25	VISa5	21	VISrl5

Allen acronym	Allen name	inter-trial commu-nity	inter-trial hub	Audio-visual cue com-mu-nity	Audio-visual cue hub
TEa2/3	Temporal association areas layer 2/3	6	VISl5	0	SSp-bfd2/3
TEa4	Temporal association areas layer 4	6	VISl5	0	SSp-bfd2/3
TEa5	Temporal association areas layer 5	21	SSs5	21	VISrl5
TEa6a	Temporal association areas layer 6a	21	SSs5	21	VISrl5
TEa6b	Temporal association areas layer 6b	8	VISli6a	-1	N/A
PERI1	Perirhinal area layer 1	-1	N/A	-1	N/A
PERI2/3	Perirhinal area layer 2/3	29	ENTl3	-1	N/A
PERI5	Perirhinal area layer 5	29	ENTl3	-1	N/A
ECT2/3	Ectorhinal area/Layer 2/3	29	ENTl3	21	VISrl5
ECT5	Ectorhinal area/Layer 5	21	SSs5	21	VISrl5
ECT6a	Ectorhinal area/Layer 6a	-1	N/A	-1	N/A
ECT6b	Ectorhinal area/Layer 6b	-1	N/A	-1	N/A
AOBgl	Accessory olfactory bulb glomerular layer	10	AON	26	ProS
AOBmi	Accessory olfactory bulb mitral layer	10	AON	26	ProS
DG-mo	Dentate gyrus molecular layer	11	DG-mo	26	ProS
DG-po	Dentate gyrus polymorph layer	11	DG-mo	26	ProS
DG-sg	Dentate gyrus granule cell layer	11	DG-mo	26	ProS
FC	Fasciola cinerea	9	CA1	-1	N/A
IG	Induseum griseum	17	SSp-ul5	1	CP
ENTl1	Entorhinal area lateral part layer 1	-1	N/A	-1	N/A
ENTl2	Entorhinal area lateral part layer 2	29	ENTl3	-1	N/A
ENTl3	Entorhinal area lateral part layer 3	29	ENTl3	11	PIR
ENTl5	Entorhinal area lateral part layer 5	9	CA1	11	PIR
ENTl6a	Entorhinal area lateral part layer 6a	-1	N/A	-1	N/A
ENTm1	Entorhinal area medial part dorsal zone layer 1	-1	N/A	-1	N/A
ENTm2	Entorhinal area medial part dorsal zone layer 2	-1	N/A	-1	N/A
ENTm3	Entorhinal area medial part dorsal zone layer 3	9	CA1	-1	N/A
ENTm5	Entorhinal area medial part dorsal zone layer 5	9	CA1	12	ANcr1
ENTm6	Entorhinal area medial part dorsal zone layer 6	9	CA1	12	ANcr1
HATA	Hippocampo-amygdalar transition area	-1	N/A	34	HATA
APr	Area prostriata	3	VISp5	7	POST
CLA	Claustrum	2	CP	2	MOp6a

Allen acronym	Allen name	inter-trial commu-nity	inter-trial hub	Audio-visual cue com-mu-nity	Audio-visual cue hub
EPd	Endopiriform nucleus dorsal part	2	CP	-1	N/A
EPv	Endopiriform nucleus ventral part	10	AON	13	BLAp
LA	Lateral amygdalar nucleus	28	COAa	14	MEA
BLAa	Basolateral amygdalar nucleus anterior part	28	COAa	-1	N/A
BLAp	Basolateral amygdalar nucleus posterior part	-1	N/A	13	BLAp
BLAv	Basolateral amygdalar nucleus ventral part	-1	N/A	-1	N/A
BMAa	Basomedial amygdalar nucleus anterior part	28	COAa	14	MEA
BMAp	Basomedial amygdalar nucleus posterior part	-1	N/A	14	MEA
PA	Posterior amygdalar nucleus	9	CA1	-1	N/A
CP	Caudoputamen	2	CP	1	CP
ACB	Nucleus accumbens	2	CP	-1	N/A
FS	Fundus of striatum	-1	N/A	14	MEA
LSc	Lateral septal nucleus caudal (caudodorsal) part	-1	N/A	3	LSr
LSr	Lateral septal nucleus rostral (rostroventral) part	18	LSr	3	LSr
LSv	Lateral septal nucleus ventral part	18	LSr	3	LSr
SF	Septofimbrial nucleus	12	SCdg	3	LSr
SH	Septohippocampal nucleus	18	LSr	3	LSr
AAA	Anterior amygdalar area	-1	N/A	-1	N/A
CEAc	Central amygdalar nucleus capsular part	-1	N/A	14	MEA
CEAl	Central amygdalar nucleus lateral part	-1	N/A	14	MEA
CEAm	Central amygdalar nucleus medial part	-1	N/A	14	MEA
IA	Intercalated amygdalar nucleus	-1	N/A	14	MEA
GPe	Globus pallidus external segment	-1	N/A	-1	N/A
GPi	Globus pallidus internal segment	28	COAa	14	MEA
SI	Substantia innominata	18	LSr	-1	N/A
MA	Magnocellular nucleus	-1	N/A	-1	N/A
MS	Medial septal nucleus	18	LSr	-1	N/A
NDB	Diagonal band nucleus	18	LSr	-1	N/A
TRS	Triangular nucleus of septum	12	SCdg	3	LSr
VAL	Ventral anterior-lateral complex of the thalamus	19	PO	17	AV
VM	Ventral medial nucleus of the thalamus	19	PO	18	MH
VPL	Ventral posterolateral nucleus of the thalamus	-1	N/A	10	APN
VPLpc	Ventral posterolateral nucleus of the thalamus parvicellular part	19	PO	10	APN

Allen acronym	Allen name	inter-trial commu-nity	inter-trial hub	Audio-visual cue com-mu-nity	Audio-visual cue hub
VPM	Ventral posteromedial nucleus of the thalamus	19	PO	10	APN
VPMpc	Ventral posteromedial nucleus of the thalamus parvicellular part	-1	N/A	18	MH
PoT	Posterior triangular thalamic nucleus	19	PO	10	APN
SPFm	Subparafascicular nucleus magnocellular part	13	MD	15	PVT
SPFp	Subparafascicular nucleus parvicellular part	-1	N/A	10	APN
SPA	Subparafascicular area	13	MD	16	SPA
PP	Peripeduncular nucleus	-1	N/A	-1	N/A
MGd	Medial geniculate complex dorsal part	9	CA1	-1	N/A
MGv	Medial geniculate complex ventral part	-1	N/A	29	LGd-co
MGm	Medial geniculate complex medial part	12	SCdg	10	APN
LGd-sh	Dorsal part of the lateral geniculate complex shell	-1	N/A	-1	N/A
LGd-co	Dorsal part of the lateral geniculate complex core	-1	N/A	29	LGd-co
LGd-ip	Dorsal part of the lateral geniculate complex ipsilateral zone	-1	N/A	29	LGd-co
LP	Lateral posterior nucleus of the thalamus	19	PO	10	APN
PO	Posterior complex of the thalamus	19	PO	10	APN
POL	Posterior limiting nucleus of the thalamus	12	SCdg	-1	N/A
SGN	Suprageniculate nucleus	19	PO	10	APN
Eth	Ethmoid nucleus of the thalamus	19	PO	-1	N/A
AV	Anteroventral nucleus of thalamus	12	SCdg	17	AV
AMd	Anteromedial nucleus dorsal part	12	SCdg	-1	N/A
AMv	Anteromedial nucleus ventral part	-1	N/A	-1	N/A
AD	Anterodorsal nucleus	-1	N/A	-1	N/A
IAM	Interanteromedial nucleus of the thalamus	12	SCdg	15	PVT
IAD	Interanterodorsal nucleus of the thalamus	12	SCdg	-1	N/A
LD	Lateral dorsal nucleus of thalamus	19	PO	10	APN
IMD	Intermediodorsal nucleus of the thalamus	13	MD	15	PVT
SMT	Submedial nucleus of the thalamus	12	SCdg	17	AV
PR	Perireunensis nucleus	12	SCdg	16	SPA

Allen acronym	Allen name	inter-trial commu-nity	inter-trial hub	Audio-visual cue com-mu-nity	Audio-visual cue hub
PVT	Paraventricular nucleus of the thalamus	12	SCdg	15	PVT
PT	Parataenial nucleus	12	SCdg	15	PVT
RE	Nucleus of reuniens	12	SCdg	15	PVT
Xi	Xiphoid thalamic nucleus	12	SCdg	15	PVT
RH	Rhomboid nucleus	12	SCdg	15	PVT
CM	Central medial nucleus of the thalamus	-1	N/A	-1	N/A
PCN	Paracentral nucleus	12	SCdg	17	AV
CL	Central lateral nucleus of the thalamus	19	PO	-1	N/A
PF	Parafascicular nucleus	22	PF	-1	N/A
PIL	Posterior intralaminar thalamic nucleus	14	APN	10	APN
RT	Reticular nucleus of the thalamus	-1	N/A	-1	N/A
IGL	Intergeniculate leaflet of the lateral geniculate complex	-1	N/A	29	LGd-co
IntG	Intermediate geniculate nucleus	-1	N/A	-1	N/A
SubG	Subgeniculate nucleus	-1	N/A	-1	N/A
MH	Medial habenula	13	MD	18	MH
LH	Lateral habenula	-1	N/A	-1	N/A
ADP	Anterodorsal preoptic nucleus	18	LSr	-1	N/A
AVP	Anteroventral preoptic nucleus	18	LSr	33	PS
MPO	Medial preoptic area	18	LSr	33	PS
PS	Parastrial nucleus	-1	N/A	33	PS
SFO	Subfornical organ	-1	N/A	3	LSr
VLPO	Ventrolateral preoptic nucleus	-1	N/A	33	PS
LM	Lateral mammillary nucleus	-1	N/A	-1	N/A
Mml	Medial mammillary nucleus lateral part	-1	N/A	-1	N/A
PH	Posterior hypothalamic nucleus	13	MD	15	PVT
LHA	Lateral hypothalamic area	12	SCdg	-1	N/A
LPO	Lateral preoptic area	-1	N/A	33	PS
PeF	Perifornical nucleus	12	SCdg	18	MH
STN	Subthalamic nucleus	25	VISa5	10	APN
TU	Tuberal nucleus	12	SCdg	10	APN
FF	Fields of Forel	-1	N/A	10	APN
SCop	Superior colliculus optic layer	3	VISp5	7	POST
SCsg	Superior colliculus superficial gray layer	3	VISp5	7	POST
SCzo	Superior colliculus zonal layer	3	VISp5	7	POST
ICc	Inferior colliculus central nucleus	1	CUN	-1	N/A
ICd	Inferior colliculus dorsal nucleus	-1	N/A	-1	N/A
ICe	Inferior colliculus external nucleus	-1	N/A	27	ICe
NB	Nucleus of the brachium of the inferior colliculus	14	APN	10	APN
SAG	Nucleus sagulum	-1	N/A	-1	N/A
PBG	Parabigeminal nucleus	-1	N/A	-1	N/A

Allen acronym	Allen name	inter-trial commu-nity	inter-trial hub	Audio-visual cue com-mu-nity	Audio-visual cue hub
SNr	Substantia nigra reticular part	14	APN	10	APN
VTA	Ventral tegmental area	14	APN	-1	N/A
RR	Midbrain reticular nucleus retrorubral area	-1	N/A	-1	N/A
SCdg	Superior colliculus motor related deep gray layer	12	SCdg	10	APN
SCdw	Superior colliculus motor related deep white layer	12	SCdg	10	APN
SCiw	Superior colliculus motor related intermediate white layer	14	APN	10	APN
PRC	Precommissural nucleus	13	MD	16	SPA
INC	Interstitial nucleus of Cajal	-1	N/A	10	APN
ND	Nucleus of Darkschewitsch	14	APN	10	APN
Su3	Supraoculomotor periaqueductal gray	-1	N/A	10	APN
APN	Anterior pretectal nucleus	14	APN	10	APN
MPT	Medial pretectal area	-1	N/A	-1	N/A
NOT	Nucleus of the optic tract	14	APN	10	APN
NPC	Nucleus of the posterior commis-sure	14	APN	10	APN
OP	Olivary pretectal nucleus	14	APN	10	APN
PPT	Posterior pretectal nucleus	14	APN	10	APN
RPF	Retroparafascicular nucleus	14	APN	10	APN
CUN	Cuneiform nucleus	1	CUN	27	ICe
RN	Red nucleus	15	RN	10	APN
III	Oculomotor nucleus	14	APN	10	APN
MA3	Medial accesory oculomotor nu-cleus	-1	N/A	-1	N/A
EW	Edinger-Westphal nucleus	-1	N/A	-1	N/A
Pa4	Paratrochlear nucleus	14	APN	10	APN
VTN	Ventral tegmental nucleus	15	RN	10	APN
AT	Anterior tegmental nucleus	16	CS	32	PRNr
DT	Dorsal terminal nucleus of the accessory optic tract	8	VISli6a	-1	N/A
MT	Medial terminal nucleus of the accessory optic tract	14	APN	-1	N/A
SNc	Substantia nigra compact part	14	APN	10	APN
PPN	Pedunculopontine nucleus	-1	N/A	-1	N/A
IF	Interfascicular nucleus raphe	15	RN	10	APN
IPA	Interpeduncular nucleus apical	14	APN	10	APN
IPL	Interpeduncular nucleus lateral	12	SCdg	-1	N/A
IPDM	Interpeduncular nucleus dorso-medial	15	RN	10	APN
IPDL	Interpeduncular nucleus dorso-lateral	14	APN	10	APN
RL	Rostral linear nucleus raphe	14	APN	10	APN
CLI	Central linear nucleus raphe	14	APN	10	APN
DR	Dorsal nucleus raphe	-1	N/A	10	APN
PSV	Principal sensory nucleus of the trigeminal	-1	N/A	28	SUT

Allen acronym	Allen name	inter-trial commu-nity	inter-trial hub	Audio-visual cue com-mu-nity	Audio-visual cue hub
KF	Koelliker-Fuse subnucleus	0	CUL4 5	9	IRN
POR	Superior olivary complex periolivary region	-1	N/A	-1	N/A
SOCm	Superior olivary complex medial part	-1	N/A	32	PRNr
SOCl	Superior olivary complex lateral part	1	CUN	-1	N/A
DTN	Dorsal tegmental nucleus	-1	N/A	-1	N/A
PDTg	Posterodorsal tegmental nucleus	-1	N/A	-1	N/A
PCG	Pontine central gray	-1	N/A	-1	N/A
PG	Pontine gray	-1	N/A	-1	N/A
PRNc	Pontine reticular nucleus caudal part	1	CUN	-1	N/A
SUT	Supratrigeminal nucleus	1	CUN	28	SUT
TRN	Tegmental reticular nucleus	16	CS	-1	N/A
V	Motor nucleus of trigeminal	-1	N/A	28	SUT
P5	Peritrigeminal zone	-1	N/A	-1	N/A
PC5	Parvicellular motor 5 nucleus	1	CUN	28	SUT
I5	Intertrigeminal nucleus	0	CUL4 5	-1	N/A
LC	Locus ceruleus	-1	N/A	-1	N/A
LDT	Laterodorsal tegmental nucleus	-1	N/A	-1	N/A
NI	Nucleus incertus	-1	N/A	-1	N/A
PRNr	Pontine reticular nucleus	-1	N/A	32	PRNr
DCO	Dorsal cochlear nucleus	0	CUL4 5	9	IRN
VCO	Ventral cochlear nucleus	0	CUL4 5	-1	N/A
CU	Cuneate nucleus	0	CUL4 5	-1	N/A
ECU	External cuneate nucleus	0	CUL4 5	9	IRN
SPVC	Spinal nucleus of the trigeminal caudal part	0	CUL4 5	9	IRN
SPVI	Spinal nucleus of the trigeminal interpolar part	0	CUL4 5	9	IRN
Pa5	Paratrigeminal nucleus	0	CUL4 5	9	IRN
VII	Facial motor nucleus	-1	N/A	-1	N/A
AMBv	Nucleus ambiguus ventral division	0	CUL4 5	9	IRN
DMX	Dorsal motor nucleus of the vagus nerve	-1	N/A	9	IRN
GRN	Gigantocellular reticular nucleus	0	CUL4 5	9	IRN
ICB	Infracerebellar nucleus	0	CUL4 5	9	IRN
IO	Inferior olivary complex	0	CUL4 5	9	IRN
IRN	Intermediate reticular nucleus	0	CUL4 5	9	IRN
LIN	Linear nucleus of the medulla	0	CUL4 5	9	IRN
LRNm	Lateral reticular nucleus magnocellular part	0	CUL4 5	9	IRN
MARN	Magnocellular reticular nucleus	0	CUL4 5	9	IRN
MDRNd	Medullary reticular nucleus dorsal part	0	CUL4 5	9	IRN
MDRNv	Medullary reticular nucleus ventral part	0	CUL4 5	9	IRN
PARN	Parvicellular reticular nucleus	0	CUL4 5	9	IRN

Allen acronym	Allen name	inter-trial commu-nity	inter-trial hub	Audio-visual cue com-mu-nity	Audio-visual cue hub
PAS	Parasolitary nucleus	0	CUL4 5	-1	N/A
PGRNd	Paragigantocellular reticular nucleus dorsal part	0	CUL4 5	9	IRN
PGRNl	Paragigantocellular reticular nucleus lateral part	0	CUL4 5	9	IRN
PRP	Nucleus prepositus	0	CUL4 5	9	IRN
LAV	Lateral vestibular nucleus	0	CUL4 5	9	IRN
MV	Medial vestibular nucleus	0	CUL4 5	9	IRN
SPIV	Spinal vestibular nucleus	0	CUL4 5	9	IRN
SUV	Superior vestibular nucleus	-1	N/A	9	IRN
x	Nucleus x	0	CUL4 5	9	IRN
XII	Hypoglossal nucleus	30	NLL	34	HATA
y	Nucleus y	0	CUL4 5	9	IRN
RO	Nucleus raphe obscurus	30	NLL	34	HATA
FN	Fastigial nucleus	0	CUL4 5	9	IRN
IP	Interposed nucleus	0	CUL4 5	9	IRN
DN	Dentate nucleus	0	CUL4 5	9	IRN
VeCB	Vestibulocerebellar nucleus	0	CUL4 5	9	IRN
MOB	Main olfactory bulb	-1	N/A	-1	N/A
AON	Anterior olfactory nucleus	10	AON	26	ProS
TTd	Taenia tecta dorsal part	-1	N/A	-1	N/A
TTv	Taenia tecta ventral part	-1	N/A	-1	N/A
DP	Dorsal peduncular area	7	DP	-1	N/A
PIR	Piriform area	-1	N/A	11	PIR
COAa	Cortical amygdalar area anterior part	28	COAa	14	MEA
COAp	Cortical amygdalar area posterior part	-1	N/A	-1	N/A
PAA	Piriform-amygdalar area	28	COAa	14	MEA
TR	Postpiriform transition area	9	CA1	13	BLAp
CA1	Field CA1	9	CA1	-1	N/A
CA2	Field CA2	9	CA1	-1	N/A
CA3	Field CA3	9	CA1	-1	N/A
PAR	Parasubiculum	-1	N/A	-1	N/A
POST	Postsubiculum	4	POST	7	POST
PRE	Presubiculum	-1	N/A	-1	N/A
SUB	Subiculum	-1	N/A	-1	N/A
ProS	Prosubiculum	9	CA1	26	ProS
OT	Olfactory tubercle	-1	N/A	-1	N/A
MEA	Medial amygdalar nucleus	-1	N/A	14	MEA
BST	Bed nuclei of the stria terminalis	18	LSr	3	LSr
MD	Mediodorsal nucleus of thalamus	13	MD	-1	N/A
LGv	Ventral part of the lateral geniculate complex	10	AON	-1	N/A
PVH	Paraventricular hypothalamic nucleus	12	SCdg	15	PVT
DMH	Dorsomedial nucleus of the hypothalamus	13	MD	15	PVT
AHN	Anterior hypothalamic nucleus	12	SCdg	15	PVT
SUM	Supramammillary nucleus	13	MD	-1	N/A

Allen acronym	**Allen name**	**inter-trial commu-nity**	**inter-trial hub**	**Audio-visual cue com-mu-nity**	**Audio-visual cue hub**
MPN	Medial preoptic nucleus	12	SCdg	15	PVT
PVHd	Paraventricular hypothalamic nucleus descending division	12	SCdg	16	SPA
VMH	Ventromedial hypothalamic nucleus	13	MD	15	PVT
MRN	Midbrain reticular nucleus	14	APN	10	APN
NLL	Nucleus of the lateral lemniscus	30	NLL	27	ICe
CS	Superior central nucleus raphe	16	CS	10	APN
NTS	Nucleus of the solitary tract	0	CUL4 5	9	IRN
SPVO	Spinal nucleus of the trigeminal oral part	0	CUL4 5	9	IRN
LING	Lingula (I)	0	CUL4 5	9	IRN
CENT2	Lobule II	0	CUL4 5	9	IRN
CENT3	Lobule III	0	CUL4 5	9	IRN
CUL4 5	Lobules IV-V	0	CUL4 5	9	IRN
DEC	Declive (VI)	0	CUL4 5	9	IRN
FOTU	Folium-tuber vermis (VII)	0	CUL4 5	9	IRN
PYR	Pyramus (VIII)	0	CUL4 5	9	IRN
UVU	Uvula (IX)	0	CUL4 5	9	IRN
NOD	Nodulus (X)	0	CUL4 5	9	IRN
SIM	Simple lobule	0	CUL4 5	9	IRN
ANcr1	Crus 1	0	CUL4 5	12	ANcr1
ANcr2	Crus 2	0	CUL4 5	9	IRN
PRM	Paramedian lobule	0	CUL4 5	9	IRN
COPY	Copula pyramidis	0	CUL4 5	9	IRN
PFL	Paraflocculus	0	CUL4 5	9	IRN
FL	Flocculus	0	CUL4 5	9	IRN